COLLECTIVE MOTION OF AN INTENSE NEUTRALIZED ION BEAM ACROSS A MAGNETIC FIELD

by

TAKASHI IKEHATA

Dissertation submitted to the Faculty of
the Graduate School of the University of Tsukuba
in partial fulfillment of the requirements for
the degree of Doctor of Science

January 1983

ABSTRACT

Conditions for cross-field propagation of a low-beta, large-gyroradius plasma have been studied experimentally by use of an intense neutralized ion beam. In particular, it is made clear that the cross-field propagation of such a plasma is caused by an $\vec{E} \times \vec{B}$ drift due to a polarization electric field and occurs when the plasma is dense enough to have a dielectric constant of greater than 100. A space-charge-neutralized and current-neutralized beam of protons with an average velocity $\bar{u}_0$ of 3.6×10^8 cm/s, a velocity spread of $0.25\bar{u}_0$, a current density of 18 A/cm^2 and a duration of 200-300 ns is produced by a reflex triode and is injected into a magnetic field $B_\perp$ of up to 3 kG applied in the direction transverse to the beam axis over a distance of about 15 cm. The beam has passed through the magnetic field without deflection. The polarization electric field E_y is observed in the beam to satisfy the relation $E_y = -\bar{u}_0 B_\perp$ which agrees with a theoretical expectation for the beam with the velocity spread. It is observed that the beam is deflected by the Lorentz force when the polarization electric field is completely short-circuited by a metal plate. This result also confirms that the polarization electric field is essential for the cross-field propagation.

CONTENTS

1. INTRODUCTION

The motion of a plasma stream across a magnetic field has been one of the most important problems of magnetohydrodynamics and has been a method of filling magnetic containment devices in thermonuclear fusion experiments with plasmas. Therefore, the cross-field propagation of plasma streams has been studied both theoretically and experimentally by many investigators.1-11) In these studies, plasma were dense enough to have the dielectric constant $\kappa = 1 + \omega_i^2/\Omega_i^2$ of 10^4-10^7 and the stream velocities ranging from 10^6 cm/s to 10^7 cm/s, where ω_i is the ion plasma frequency and Ω_i is the ion gyrofrequency. The common result from those experiments was the penetration of the plasma into the magnetic field over a distance much longer than the ion gyroradius ρ_i. Of course, this result can not be explained from the simple single-particle picture since individual particles of the plasma injected into the magnetic field can not travel further than one to two gyroradii without interparticle collisions. Therefore, some collective interactions between the plasma and the magnetic field have to be expected. Candidates for the collective interactions are as follows:

1) the interaction concerned with the plasma diamagnetism,
2) the interaction associated with an electric field generated by the plasma.

In the most of those experiments, the plasma kinetic pressure is small compared with the pressure of the magnetic field (low β), that is,

$$\frac{1}{2} m_i n u^2 < \frac{B_\perp^2}{2\mu_0} , \tag{1}$$

so that the diamagnetic effect can not explain this collective penetration of the plasma into the magnetic field, where m_i is the ion mass, n the plasma density, u the stream velocity, $B_\perp$ the component of the magnetic field perpendicular to the stream and μ_0 is the permeability of vacuum.1-5,11) (It is well known that the plasma excludes the magnetic field from its interior and penetrates a transverse magnetic field when the plasma is completely diamagnetic and satisfies the condition $m_i n u^2/2 > B_\perp^2/2\mu_0$.6-8) In our study, however, this effect is not important because the condition (1) is well satisfied.)

Schmidt12) first developed a theoretical model for the non-diamagnetic motion of a plasma stream in a curved magnetic field, under assumptions that the plasma is dense enough to be $\kappa >> 1$ and the motion of plasma particles satisfies the adiabatic condition13)

$$\frac{1}{B} \left| \frac{dB}{dt} \right| \Big/ \Omega << 1.$$

He used the guiding center approximation to describe the motion of plasma particles and a self-consistent field treatment to describe the electromagnetic field generated by the plasma. The above condition of $|dB/dt|/B\Omega << 1$ can be expressed for the stationary field as

$$u\Omega^{-1} << B/|\vec{\nabla}B|. \qquad (2)$$

Equation (2) indicates that the adiabaticity of motion of a plasma particle is assured only when a distance traveled by the particle in one gyroperiod Ω^{-1} is much smaller than the scale length of spacial variation in the magnetic field strength B. The use of the guiding center approximation is justified as long as the adiabatic condition (2) is satisfied. The model of Schmidt predicted the rectilinear motion of the plasma in the curved magnetic field by the following mechanism: As the plasma with the velocity $\vec{u}$ enters a curved region of the magnetic field $\vec{B}$, guiding centers of ions and electrons shift due to the curvature and grad-B drifts in opposite directions to each other, perpendicular to both directions of the velocity $\vec{u}$ and the transverse component $\vec{B}_\perp$ of the magnetic field $\vec{B}$. These shifts of guiding centers give rise to the accumulation of ions and electrons on plasma boundaries of opposite sides to each other and induce an electric field $\vec{E}$ in the plasma in the direction opposite to the Lorentz force $q\vec{u} \times \vec{B}$. Such a charge separation of the plasma is often called polarization and the induced electric field called the polarization electric field. The polarization electric field $\vec{E}$ then makes it possible for the plasma to move straight irrespective of the curvature of the magnetic field by means of the $\vec{E} \times \vec{B}$ drift. The drift velocity of the plasma is kept equal to its initial velocity $\vec{u}$ as long as the condition $\kappa >> 1$ is satisfied.

There are two types of plasmas which are used in the study on cross-field propagation of plasma streams. The one is the plasma which has been produced with a variety of plasma guns and has been used in studies so far. The other is the plasma as an intense neutralized ion beam14) which is used in the present study.

The intense neutralized ion beam is a new type of ion beam which has been developed rapidly since its first discovery15) in 1974. This beam has the following features which are not seen in conventional ion beams: First, the intense neutralized ion beam has a large electrical power of 10^8-10^{12} W and a short duration of 100-500 ns. The ion energy of a few MeV and the beam current of several hundred kA have already been achieved.16) Second, the intense neutralized ion beam is space-charge and current neutralized by electrons dragged along from the beam source. The charge neutrality of the beam means that the beam is composed of ions and electrons with the same number density so that no electric field of the space charge exists in the beam. Then, the beam can propagate in vacuum without the significant expansion caused by the electric field. The current neutrality of the beam means that ions and electrons in the beam have the same velocity so that the beam does not carry a net current. In these senses, the beam can be regarded as a plasma stream with a large forward momentum. We shall

Table I. Comparison between the intense neutralized ion beam and the gun-produced plasma as the means to study the cross-field propagation of plasma streams.

	Stream velocity	Number density	Radial divergence	Axial velocity spread	Adiabaticity of motion of particles	Condition $\kappa >> 1$
Intense neutralized ion beam	10^8-10^9 (cm/s)	10^{11}-10^{13} (cm^{-3})	Small	Small ($\Delta u_0 << \bar{u}_0$)	Not satisfied	Marginally satisfied
Gun-produced plasma	10^6-10^7 (cm/s)	10^{12}-10^{17} (cm^{-3})	Large	Large ($\Delta u_0 \gtrsim \bar{u}_0$)	Satisfied	Well satisfied

however, stick to the term ion beam because of the way the beam is produced. The intense neutralized ion beam is produced with an ion diode coupled to a Marx generator.17) The ion diode is a vacuum diode composed of an anode of plastic and a cold cathode. By the application of a positive high voltage to the anode from the Marx generator, the anode is ionized and is covered with a dense plasma. Ions in the plasma are then accelerated outward and form an ion beam. In general, some designs are performed to the ion diode to improve the efficiency of ion beam production.14,15,16,18-20) The properties of the intense neutralized ion beam are compared with those of the gun-produced plasma in Table I.

Intense neutralized ion beams, because of their features described above, present new approaches to realize thermonuclear fusion reactors such as,

1) inertial fusions drived by ion beams,14,21,22)
2) reverse-field ion rings or layers,14,23-25)
3) the rapid heating of magnetically confined plasmas.14,26,27)

Among them, the applications to magnetic confinement fusions, for example, to the formation of reverse-field ion rings are attractive since reverse-field ion rings have a possibility of realizing compact and economical fusion reactors.23)

The present paper reports results of the experiment which studies the collective motion of an intense neutralized ion beam across a magnetic field.28,29) The use of the intense neutralized ion beam instead of the gun-produced plasma to study the cross-field propagation of plasma streams has substantial meanings coming from differences in their properties shown in Table I: First, the intense neutralized ion beam is more advantageous to study the cross-field propagation than the gun-produced plasma. The reason for this is that the radial divergence and the axial velocity spread of the particles are small in the intense neutralized ion beam compared with those in the gun-produced plasma, so that this beam is regarded as a nearly one-dimensional stream of a cold plasma. Such a plasma stream can be well analyzed with the help of a simple one-dimensional model. Second, the adiabatic condition (2) and the condition $\kappa >> 1$ are well satisfied in studies carried out with use of gun-produced plasmas, so that the result of those studies, that is, the penetration of the plasma through the magnetic field is successfully explained with the model of Schmidt. In the intense neutralized ion beam, on the other hand, the adiabatic condition is not satisfied at all because of large gyroradii of the ions so that the adiabatic model of Schmidt can not be applied any longer.

It has already been verified in our previous study that the intense neutralized ion beam can propagate across the magnetic field without deflection but the mechanism of the propagation has not been identified.30,31) In the present paper, observation of the polarization electric field in the intense neutralized ion beam is described in detail, which is very important to identify the mechanism of the propagation of the beam across the magnetic field. As a result of the present study, in particular, it is made clear that the beam passes through the magnetic field by means of the $\vec{E} \times \vec{B}$ drift due to the polarization electric field $\vec{E}$ in the beam when the condition $\kappa \geq 100$ is satisfied. Theoretical models have been developed by Sinelnikov and Rutkevich$^{32)}$ and independently by Peter and Rostoker$^{33)}$, which analyze the non-adiabatic motion of a plasma injected into a transverse magnetic field and meet our experimental condition. They used one-dimensional two-fluid equations including a self-consistent electric field to describe the motion of the plasma and assumed that the transverse magnetic field rose rapidly from zero to a spacially constant value at the field boundary. Their models predicted the undeflected propagation of the plasma across the magnetic field by the same mechanism as in the adiabatic model of Schmidt (that is, the $\vec{E} \times \vec{B}$ drift due to the polarization electric field). In particular, Peter and Rostoker$^{33)}$ showed that the condition for cross-field propagation of the plasma now became $\kappa \gg (m_i/m_e)^{1/2}$ stronger than $\kappa \gg 1$ in the adiabatic case because of the failure in the adiabaticity of motion of plasma particles at the field boundary. It should be noted that this condition of $\kappa \gg (m_i/m_e)^{1/2}$ is written as $\kappa \gg 43$ for a hydrogen plasma as in our case. Results of the present study show good agreement with theoretical predictions of their models. Effects of a metal plate placed in the magnetic field on the propagation of the beam are also studied since it is anticipated that the metal plate short-circuits the polarization electric field in the beam; the short circuit of the polarization electric field is found to occur only when the metal plate is placed so as to come in contact with the beam; then, the beam is deflected according to single-particle orbits of beam ions under the Lorentz force. These results of the present study indicate that the direct injection of intense neutralized ion beam into a magnetic field across the field lines (cross-field injection) is promising as a method of creating reverse-field ion rings or heating magnetically confined plasmas. In Section 2, a simplified model of cross-field propagation of the beam is presented. The experimental apparatus and diagnostic tools are described in Section 3. Experimental results are given in Section 4. Section 5 is devoted to the discussion of the results. Concluding remarks are presented in Section 6.

2. THEORETICAL MODEL

We consider the motion of an intense neutralized ion beam as a plasma stream across a magnetic field, using a simplified model shown in Fig. 1. A uniform magnetic field $B_\perp$ oriented to +x is applied in the region $z \geq 0$. A beam, composed of ions and electrons with the same velocity u_0 and density n_0, enters the magnetic field at $z = 0$. The beam is bounded in the y direction and is extended infinitely in the x direction. Ions and electrons of the beam are deflected to opposite directions to each other along the y axis by the Lorentz force. Ions accumulate on the upper boundary (+y direction) of the beam and produce a positive charge layer, while electrons accumulate on the lower boundary (-y direction) and produce a negative charge layer. These positive and negative charge layers are responsible for the polarization electric field E_y in the direction transverse to the beam axis. The accumulation of charges continues until the electric force due to the polarization electric field and the Lorentz force are balanced. This electric field E_y in turn makes the beam propagate across the magnetic field by means of the $\vec{E} \times \vec{B}$ drift.

The model equations have been developed and solved by Sinelnikov and Rutkevich,32) and independently by Peter and Rostoker.33) The model equations are composed of the equations of motion and the equations of continuity for ions (subscript i) and electrons (subscript e) and are given in the form

$$\frac{\partial}{\partial t}\vec{v}_i + (\vec{v}_i\cdot\vec{\nabla})\vec{v}_i = \frac{e}{m_i}(\vec{E} + \vec{v}_i\times\vec{B}) + \frac{m_e}{m_i}\nu(\vec{v}_e - \vec{v}_i), \quad (3)$$

$$\frac{\partial}{\partial t}\vec{v}_e + (\vec{v}_e\cdot\vec{\nabla})\vec{v}_e = -\frac{e}{m_e}(\vec{E} + \vec{v}_e\times\vec{B}) - \nu(\vec{v}_e - \vec{v}_i), \quad (4)$$

$$\frac{\partial}{\partial t}n_i + \vec{\nabla}\cdot(n_i\vec{v}_i) = 0, \quad (5)$$

$$\frac{\partial}{\partial t}n_e + \vec{\nabla}\cdot(n_e\vec{v}_e) = 0, \quad (6)$$

where $\vec{v}_j = (0, v_j, u_j)$ and n_j are the velocity vector and the density of ions ($j = i$) and electrons ($j = e$), m_i (m_e) the ion (electron) mass, e the elementary charge and ν is the effective collision frequency between ions and electrons. In eqs. (3) and (4), $\vec{E} = (0, E_y, E_z)$ is the polarization electric field and $\vec{B} = (B_\perp, 0, 0)$ is the magnetic field applied externally. Here, we confine ourselves to the steady-state solutions of the model equations (3)-(6), following Sinelnikov and Rutkevich's approach. This means from eqs. (5) and (6) that the ion and electron currents are taken to be independent of time. Then, all physical variables, such as velocity and density, are regarded as a function of z only. The complete description of the general solutions of eqs. (3)-(6) will appear in Appendix A.

In the limiting case of $\nu = 0$, eqs. (3)-(6) reduce to

$$u \frac{dv}{dz} = \frac{e}{m_e} E_y + \Omega_e u, \tag{7}$$

$$u \frac{du}{dz} = -\Omega_i v, \tag{8}$$

$$v = v_i - v_e, \tag{9}$$

$$u = u_i = u_e = u_0 (n_0/n),/n), \tag{10}$$

where $\Omega_i = eB_\perp/m_i$ and $\Omega_e = eB_\perp/m_e$. In eqs. (7)-(10), the quasi-neutrality of the beam ($n_i = n_e = n$) in the magnetic field is assumed and terms of order $m_e/m_i << 1$ are neglected. We can solve eqs. (7)-(10) for $1 - u/u_0 << 1$ by substituting E_y of the form

$$E_y = -\frac{en}{\varepsilon_0} \delta y, \tag{11}$$

where ε_0 is the permittivity of vacuum and $\delta y = y_i - y_e$ is the relative displacement of ions to electrons in the y direction. As a result, the beam velocity u is derived as

$$u = u_0 [1 - \frac{1}{\kappa}(1 - \cos\frac{\sqrt{\kappa} z}{\rho_h})], \tag{12}$$

the relative displacement δy is given by

$$\delta y = \frac{\rho_i}{\kappa}(1 - \cos\frac{\sqrt{\kappa} z}{\rho_h}), \tag{13}$$

and the polarization electric field E_y becomes

$$E_y = -u_0 B_\perp \left(1 - \cos\frac{\sqrt{\kappa} z}{\rho_h}\right)\left(1 - \frac{1}{\kappa}\cos\frac{\sqrt{\kappa} z}{\rho_h}\right), \tag{14}$$

where $\kappa = 1 + \omega_i^2/\Omega_i^2$ is the dielectric constant of the beam, $\rho_i = m_i u_0/eB_\perp$ the ion gyroradius, $\rho_e = m_e u_0/eB_\perp$ the electron gyroradius and $\rho_h = (\rho_i \rho_e)^{1/2}$ is the hybrid gyroradius. Equations (12)-(14) are illustrated in Fig. 2. After averaging out the spacial oscillations in eqs. (12)-(14), we obtain

$$u = u_0\left(1 - \frac{1}{\kappa}\right), \tag{15}$$

$$\delta y = \frac{\rho_i}{\kappa}, \tag{16}$$

$$E_y = -u_0 B_\perp \left(1 + \frac{1}{2\kappa}\right). \tag{17}$$

In the case of $\nu > 0$, it is shown that the spacial oscillations observed in eqs. (12)-(14) are damped out in a distance $z \gtrsim 2u_0/\nu$ or are suppressed completely. Then, u, δy and E_y approach asymptotically the values given by eqs. (15)-(17), respectively (Appendix A).

From eqs. (15)-(17), the following conclusion is derived: In the limit of large κ, the polarization electric field $E_y = -u_0 B_\perp$ is set up in the beam and cancels out the Lorentz force, and the beam can propagate undeflected across $B_\perp$ with its initial velocity u_0 by means of the $\vec{E} \times \vec{B}$ drift.

This conclusion is valid only when the quasi-neutrality assumption $n_i = n_e$ holds. The validity of the assumption is checked in Section 5, where it is shown that the condition of κ stronger than $\kappa \gg 1$ must be satisfied for the quasi-neutrality of the beam to be preserved in the magnetic field $B_\perp$.

Effects of the beam thickness in the y direction on the propagation of the beam can not be treated in the above model since this model is one-dimensional and takes all physical variables as a function of z only. A more complete model in which the velocity and density of the beam are treated as functions of both y and z is necessary to investigate these effects. Such a two-dimensional treatment is often difficult to do analytically. Here, we derive requirements to the beam thickness from simple considerations, assuming $\kappa \gg 1$. First, the thickness of the polarization charge layers $\delta y = y_i - y_e$ must be much smaller than the beam thickness w to keep the bulk of the beam charge-neutral, so that $\delta y \ll w$. From eq. (16), this requirement can be expressed as

$$w \gg \frac{\rho_i}{\kappa} . \tag{18}$$

Equation (18) gives a lower limit on the beam thickness. Next, the potential difference between the positive and negative charge layers should not exceed the initial energy of beam ions. This leads to $eE_y w < m_i u_0^2/2$, or from eq. (17), to

$$w < \frac{1}{2} \rho_i \quad . \tag{19}$$

Equation (19) shows an upper limit on the beam thickness. (The applicability of eq. (19) still leaves room for discussion from the side of experiment.34))

3. EXPERIMENTAL APPARATUS

A schematic drawing of the experimental apparatus is shown in Fig. 3. For convenience, we define the coordinate system x, y, z as shown in the figure. The intense neutralized ion beam is produced by a reflex triode 18) coupled to a Marx generator. The Marx generator can store the energy of 2.2 kJ in maximum and generate the open voltage of 400 kV in maximum in the positive polarity. The output of the Marx generator is directly connected to the anode and no pulse forming line is used. The anode (the source of beam ions) is a thin Mylar sheet of 4 μm in thickness and 3 cm in diameter. The cathode, made of stainless steel, has a diameter of 2.5 cm and is placed at 2 cm apart from the anode. A pin made of stainless steel (a cathode pin) is attached on the cathode to accelerate the production of the anode plasma. An axial magnetic field B_z of 6 kG is applied to the triode by the discharge of a capacitor bank to eliminate the electron loss to the anode support and to make the beam production reproducible. The triode region is surrounded by a thin, stainless-steel sheet which is electrically grounded.

The beam extracted from the anode propagates about 50 cm downstream in a vacuum vessel. An aperture, 2.5 cm in diameter and made of stainless steel, is placed in the vacuum vessel at 35 cm downstream from the anode to prevent the contact of the beam with the vessel wall. The vacuum vessel is composed of Pyrex tubes with a diameter of 10 cm and is evacuated down to 2 x 10^{-5} Torr (2.7 x 10^{-3} Pa) by oil diffusion pumps before each shot. The transverse magnetic field $B_\perp$ which has the strength of up to 3 kG at the center of the $B_\perp$ region ($x = y = z = 0$) and the duration of 10 ms is produced by a pair of mirror coils energized by a capacitor bank. The strength of $B_\perp$ is constant within an accuracy of about 10 % in the region $-4 \leq x \leq 3$ cm and $-5 \leq z \leq 5$ cm as shown in Fig. 4. The time sequence is adjusted so that the Marx generator may be fired at the peak of B_z and $B_\perp$ fields.

Diagnostic tools used in the present experiment are as follows:

Copper-sulphate voltage divider

The anode voltage is attenuated by a combination of a copper-sulphate divider and a high-tension resistive divider and is displayed on an oscilloscope. The copper-sulphate divider consists of a plastic cylinder filled with copper-sulphate solution, in which a disc electrode made of copper is immersed to pick up the voltage drop in the solution. One end of the cylinder is connected to the output of the Marx generator and the other end is grounded. The time response (less than 10 ns) and the attenuation ratio (1 to 3.1 x 10^4) of dividers are calibrated for square pulses with a 100-ns duration and a few nano-second rise time (pulse generator: HP 8015A).

Rogowski coil

A Rogowski coil is set around the cathode support to measure the diode current. The output of the coil is terminated by a low-inductance shunt resistor made of titanium ribbon. The signal is self-integrated by a RL-integrating circuit composed of the coil inductance L and the resistance R of the shunt. This self-integrating Rogowski coil is found superior to a popular, RC-integrating Rogowski coil in the measurement of strong and rapidly varying currents because in the former the coil inductance L serves as an element of the integrator, while in the latter the inductance L degrades the time response of the coil. The Rogowski coil is calibrated by measuring an oscillating current with the known strength and frequency.

One-turn loop

Signals from one-turn loops are fed to RC-integrating circuits with a time constant of 100 ms to measure the strength of B_z and $B_\perp$ fields.

Magnetic analyzer

A 180° deflection magnetic analyzer is used to give momentum spectra of beam ions. The analyzer is equipped with an entrance slit (0.3 cm in width) and fifteen Faraday cups (0.75 cm in diam.) as detectors. Faraday cups are arrayed at intervals of 1 cm. The momentum resolution is less than 5 %. A neutral pressure in the analyzer is kept below

5×10^{-5} Torr (6.7×10^{-3} Pa).

Langmuir probe

The polarization electric field in the beam is measured by a pair of special Langmuir probes. Schematic drawing of the probe is shown in Fig. 5. The probe contains resistors, a series of ten resistors of 6 kΩ and a 50-Ω termination resistor, in a Pyrex sleeve with a diameter of 1.2 cm. The potential picked up by the small electrode (0.05 cm in diam.) of the probe is divided by the resistors (50 Ω/60 kΩ) and is displayed on an oscilloscope. The use of insulator instead of metal as the sleeve material is essential to reduce the input capacitance of the probe and therefore to improve the frequency response of the probe. To investigate whether the probe really measures the floating potential in the beam, the input resistance of 60 kΩ was decreased to 10 kΩ. If the probe measured the saturation current, the signal (the potential on the probe electrode) for 10 kΩ would be 1/6 of that for 60 kΩ. The signal, however, reduced by only 10 % when the resistance was decreased from 60 kΩ to 10 kΩ. Therefore, the input resistance of 60 kΩ is sufficient to measure the floating potential in the beam.

Calorimeter

Total beam energy is inferred from the increase of temperature of a thin copper disc (8.4 cm diam. x 0.01 cm) by the exposure to the beam. The increase of temperature is detected by a copper-constantan thermocouple attached on the center of the disc. The heat capacity of the disc is 1.9 J/K.

Charge collector

Charge collectors are utilized to measure the ion current density. The basic structure of the charge collector is shown in Fig. 6, together with a bias circuit. (The charge collector of this type has been called S.E.D so far.) A mesh detector made of stainless steel and with a transparency T of 0.6 is located in a shield case. A grounded mesh (T = 0.6) is placed in front of the detector at a distance of 0.5 cm. The shield case and the grounded mesh are also made of stainless steel. A negative bias of -300 V is applied to the detector through the bias circuit to repell electrons dragged by the ions. Charges entering into the detector flow through a load resistor (1 Ω). The voltage drop on the resistor is fed to an oscilloscope as the signal.

To measure radial profiles of the ion current density, a 7-channel charge collector in which mesh detectors are set in array at intervals of 1.2 cm is used. Four signals from seven detectors are observed simultaneously at one firing of the beam. A single-channel charge collector (T = 0.6, 2.5 cm in diam.) is employed to infer the beam velocity from the time-of-flight method. The net current density (the sum of ion and electron current densities) is also measured with use of this device. Then, the bias voltage to the detector is set to zero.

A possibility that secondary electrons emitted from the detector by bombardment with the ions contribute considerably to the signal, can be denied from the following argument: A transverse magnetic field $B_\perp$ used in the present experiment also serves to suppress the flow of secondary electrons from the detector by magnetic insulation. The critical strength B_c of the magnetic field required for the insulation of the electrons is given by

$$B_c = d^{-1}(2m_eV/e)^{1/2}[1 + (eV/2m_ec^2)]^{1/2}, \qquad (20)$$

where d is the spacing between the detector and the outer shield case and V is the bias voltage.[19)] When typical parameters, d = 0.5 cm and V = 300 V are substituted to eq. (20), we obtain B_c = 120 G. This value is easily achieved in the present experiment by use of the $B_\perp$ field.

In the absence of $B_\perp$, the secondary electron current can be limited by the Child-Langmuir law to the negligible level (space-charge-limited current). All the bias circuits of charge collectors are calibrated for square pulses with a duration of 200 ns and a rise time of a few nano seconds (pulse generator: HP 8015A).

Framing camera

Framing pictures of the light from the anode plasma are taken by use of a image converter camera (Hadland Photonix, IMACON 790) to investigate the time evolution of the anode plasma. A photocathode (S-20) of the camera is sensitive to the light with a wavelength over the range 0.3-0.8 μm (maximum sensitivity at 0.42 μm). The operation of the camera is triggered by the anode voltage. Immediately after a certain delay from the trigger, the shutter is opened and a series of events around the anode are recorded on a film (Polaroid T-410) at the framing speed of 2 x 10^7 frames per second. The number of frames recorded on the film is adjustable from 8 to 16. The delay time can be adjusted so that the camera may operate in the period of the anode plasma formation of interest.

Signals from these diagnostic devices are observed with two dual-beam oscilloscopes (Tektronix 7844) and a storage oscilloscope (Tektronix 7834) in a screen room and are recorded on films (Polaroid T-410) of attached cameras (Tektronix C-51 and C-27). All the signal cables (3D2W) have the same length (20 m) within an accuracy of less than 50 cm.

4. EXPERIMENTAL RESULTS

A. Production of the ion beam

Characteristics of the reflex triode and the ion beam extracted were investigated. The reflex triode was operated at an output voltage of 260 kV of the Marx generator. Oscillograms of the anode voltage and the diode current are shown in Fig. 7. The anode voltage rises rapidly to 200 kV in less than 40 ns after the firing of the Marx generator and stays at this value for 150 ns (high impedance phase). In this period, the diode current is less than 1 kA. Simultaneously with a sudden fall in the anode volatge to 100 kV, the diode current starts to rise. While the diode current increases to its peak value of 15 kA in 250 ns after its rise, the anode voltage decreases gradually and comes to zero at the peak of the diode current (ion flow mode). Signals of the anode voltage and the diode current were reproduced within an accuracy of 10 %. A more detailed study of the reflex triode, including framing photography of the anode plasma, is described in Appendix B.

The time-of-flight method was applied to measure the velocity of the ion beam. The ion current detected by a charge collector on the z axis rose up linearly to its peak in 200 ns and decayed linearly to zero in 200-300 ns thereafter. The peak of the ion current propagated at a velocity of (3.4-4.1) x 10^8 cm/s. The emission time of beam ions from the anode was found to occur during the ion flow mode.

Figure 8 shows radial profiles of the ion current density observed at $z = 0$. The beam has an ion current density of 18 A/cm^2 at the peak and a circular cross section of 5.0 cm FWHM in diameter. A half divergence angle of the beam is calculated to be 4° from the observation that the diameter of the beam increases from 2.5 cm to 5.0 cm in the course of propagation from $z = -35$ cm to $z = 0$. The total ion current is calculated from Fig. 8 to be 350 A. The net current density at $z = 0$ on the z axis was about 4 A/cm^2. From these facts that the beam propagates a distance of 50 cm without the significant loss of the ions and the net current density of 4 A/cm^2 is about 1/5 of the ion current density of 18 A/cm^2, the beam is inferred to be space-charge-neutral and almost current-neutral.

Momentum analysis of beam ions by means of the magnetic analyzer showed that momentums of the ions were ranging from 4.6×10^{-19} kg·cm/s to 7.5×10^{-19} kg·cm/s at the peak of the ion current. Combined with data from the time-of-flight measurement, this shows that the ions are dominated by protons. Other ion species constituting the anode, that is, carbon and oxygen were not detected in the beam. Once components of beam ions are identified, we can obtain a velocity distribution function of the ions from data of momentum analysis. The result is shown in Fig. 9. The distribution is nearly a shifted Maxwellian with the average

Table II

Typical beam parameters.

Ion species	Proton
Average velocity of ions	3.6×10^8 cm/s
Velocity spread of ions	0.9×10^8 cm/s
Ion current density (peak)	18 A/cm^2 at $z = 0$ 11 A/cm^2 at $z = 6$ cm
Half divergence angle of the beam	4°
Diameter of the beam	5.0 cm FWHM at $z = 0$
Duration of the beam	200-300 ns FWHM

velocity $\bar{u}_0$ of 3.6 x 10^8 cm/s (which is equivalent to 70 keV in energy) and with the velocity spread Δu_0 of 0.9 x 10^8 cm/s. This distribution appeared not to vary within the diameter of the beam because ion currents observed at different radii started to rise and reached their peaks at the same time. Parameters of the beam are listed in Table II.

B. Propagation of the beam across a magnetic field

(i) Undeflected penetration into the magnetic field

The ion beam was injected along the z axis into the transverse magnetic field $B_\perp$ of up to 3 kG applied in the +x direction. By the application of $B_\perp$, signals from charge collectors suffered high frequency noises with frequencies around 30 MHz. Amplitudes of noises increased with increasing the $B_\perp$ strength, while those of signals decreased with increasing the $B_\perp$ strength. Electrostatic shielding of signal cables was done carefully to eliminate noises; all signal cables were bundled together and were put in a copper pipe with a thickness of 0.2 cm. As a result of the shielding, we could obtain reliable data even at $B_\perp$ = 3 kG.

Radial profiles of the ion current density of the beam observed at z = 0 and z = 6 cm for $B_\perp$ = 2 kG are shown in Figs. 10 and 11, respectively. If only the Lorentz force acted on the ions, the beam would be deflected and the peak of the ion current density would shift to y = 4.6 cm (at z = 6 cm for $B_\perp$ = 2 kG). The significant shift of the current peak is, however, not observed in Fig. 11 and was not observed for $B_\perp$ = 3 kG either. The reason for this is that the electric field is formed in the beam along the y axis by the polarization, which makes the beam go straight across $B_\perp$ by the $\vec{E} \times \vec{B}$ drift.

Figures 10 and 11 also show that the beam expands along $B_\perp$ field lines in the course of propagation. The width of the profile along $B_\perp$ field lines is increased from 6 cm FWHM to 9 cm FWHM with increasing the axial distance from z = 0 to z = 6 cm, while that transverse to $B_\perp$ field lines remains 4.0-4.5 cm FWHM independent of the axial distance. This means that the cross section of the beam is deformed to ellipse from circle (5.0 cm in diam.) at $B_\perp$ = 0. The expansion of the beam was not so apparent at $B_\perp$ = 1 kG as at $B_\perp$ = 2 kG. In this case, the width of the profile of the ion current density was 4.5 cm FWHM at z = 0 and 5.5 cm FWHM at z = 6 cm along $B_\perp$ field lines, while it was 4 cm FWHM at z = 0 and 4.5 cm FWHM at z = 6 cm across $B_\perp$ field lines. As a result, the expansion of the beam increased with increasing the $B_\perp$ strength or the axial distance to be traversed. This phenomenon had been also observed in the previous experiment,30,31) where the reduction in the ion current density in the magnetic field $B_\perp$ had been studied in connection with the expansion of the beam.

The process leading to the expansion is explained qualitatively as follows: As a cylindrical beam enters the magnetic field $B_\perp$, the component E_x of the polarization electric field along $B_\perp$ field lines is induced on the surface of the beam. This situation is illustrated in Fig. 12. Ions and electrons on the surface are freely accelerated outward from the beam along the field lines by E_x. On the other hand, the electrostatic force qE_y and the Lorentz force $qu_0B_\perp$ are balanced in the direction transverse to $B_\perp$ field lines and the acceleration of ions and electrons in this direction does not occur. As a whole, the beam expands only in the direction of the $B_\perp$ field.

(ii) Formation of the polarization electric field

To identify the mechanism of the beam propagation, observation of the polarization electric field is essential. When the beam has the velocity spread of the ions, the expression of the polarization electric field differs from $E_y = -u_0B_\perp$ and is derived as follows: The drift velocity $u_d = -E_y/B_\perp$ of the plasma stream in which the velocity spread of the ions is not so large compared with the drift velocity as in our case, is given in ref. 5 as

$$u_d = \bar{u}_0 \frac{m_i n}{\varepsilon_0 \kappa B_\perp^2} , \tag{21}$$

where κ is exactly of the form

$$\kappa = 1 + \frac{\omega_e^2}{\Omega_e^2} + \frac{\omega_i^2}{\Omega_i^2} . \qquad (22)$$

In eq. (22), ω_e^2/Ω_e^2 is smaller than ω_i^2/Ω_i^2 by a factor of m_e/m_i and can be neglected. For cases of interest, $\omega_i^2/\Omega_i^2 >> 1$. As a result, eq. (21) reduces to $u_d = \bar{u}_0$ and the polarization electric field to be observed is expressed as

$$E_y = -\bar{u}_0 B_\perp . \qquad (23)$$

A pair of Langmuir probes at floating potential was inserted into the beam to measure the polarization electric field directly. The upper and lower probes are located at y = 1.0 cm and y = -0.5 cm on the y axis, respectively. The electric field E_y was evaluated from the potential difference $\Delta\phi$ between the probes and the probe separation Δy as

$$E_y = -\Delta\phi/\Delta y .$$

A signal of floating potential detected by each probe rose to its peak in 100-150 ns after the arrival of the beam front and decayed to zero within the duration of the beam (300-400 ns). In the absence of $B_\perp$, signals from the upper and lower probes were identical and indicated the presence of a uniform potential of about 500 V within the diameter of the beam. On the other hand, the signal from the upper probe was superior in amplitude to that from the lower probe whenever $B_\perp$ was applied in the +x direction. This shows the presence of an electric field in the -y direction. This direction of the electric field is opposite to that of the Lorentz force acting on the ions, as predicted by the theory.

Typical oscillograms of the electric field E_y, together with the oscillogram of the ion current pulse, are shown in Fig. 13. (Throughout the present paper, we adopt as the typical value of the electric field the one at the time when the ion current reaches its peak [5].) The strength $E = |E_y|$ of the electric field E_y increases linearly from 3.6 kV/cm to 7.5 kV/cm with increasing the $B_\perp$ strength from 1 kG to 2 kG ([2] and [3]) and is null at $B_\perp = 0$ ([1]). The direction of the electric field reverses on reversal of the direction of $B_\perp$, but its strength does not change ([4]). The oscillatory behavior of the electric field E_y appearing in eq. (14) was not observed in the present experiment. The reason for this is not clear yet; however, we suspect that effective collisions between ions and electrons or the phase mixing due to the velocity spread of ions is responsible for this.35) (See also Appendix A.)

Figure 14 shows the electric field strength E as a function of the $B_\perp$ strength. The solid line in the figure represents the strength of the polarization electric field, $E = \bar{u}_0 B_\perp$ predicted theoretically from eq. (23) for $\bar{u}_0 = 3.6 \times 10^8$ cm/s. Agreement between the experimental result and the theoretical prediction is good. Therefore, it can be concluded that the mechanism of the cross-field propagation of the beam with the velocity spread is the

$\vec{E} \times \vec{B}$ drift of the ions and electrons by the polarization electric field $E_y = -\bar{u}_0 B_\perp$. The dielectric constant κ of the beam was evaluated at $z = 0$ from ion current densities and $\bar{u}_0 = 3.6 \times 10^8$ cm/s to be 2300 ($B_\perp = 1$ kG), 500 ($B_\perp = 2$ kG) and 140 ($B_\perp = 3$ kG).

(iii) Distribution of the polarization electric field along $B_\perp$ field lines

The distribution of the electric field strength E in the beam along $B_\perp$ field lines was measured by the scan of the probes along the x axis. The results are presented in Fig. 15 for $B_\perp = 1$ kG and $B_\perp = 2$ kG. In the figure, solid lines denote theoretical distributions of $E = \bar{u}_0 B_\perp$ and are calculated from $\bar{u}_0 = 3.6 \times 10^8$ cm/s and the profile of the $B_\perp$ strength on the x axis shown in Fig. 4. The strength of $B_\perp$ is not constant along the x axis (except for the vicinity of $x = 0$) but monotonically increases with increasing $|x|$ since $B_\perp$ is produced by mirror coils.

In the region $x \leq 4.5$ cm, the electric field is formed in the beam so as to satisfy locally the relation $E = \bar{u}_0 B_\perp$ in accordance with the spacial variation in the $B_\perp$ strength for both cases of $B_\perp = 1$ kG and $B_\perp = 2$ kG. In the region $x > 4.5$ cm, on the other hand, the electric field strength decreases rapidly in spite of the increase in the $B_\perp$ strength and is far below that required for the propagation of the beam. The ion current was detected in the region $x > 4.5$ cm as well as in the region $x \leq 4.5$ cm though its intensity decreased with increasing x.

C. Cross-field propagation of the beam near a metal plate

Effects of a metal plate which is set perpendicular to $B_\perp$ field lines on the propagation of the beam across the magnetic field $B_\perp$ were investigated. The metal plate made of stainless steel (0.01 cm thick x 12 cm wide x 9 cm high) was placed in the vacuum vessel with its surface parallel to the beam axis and perpendicular to $B_\perp$ field lines. Except for the metal plate, the experimental arrangement is not changed from Fig. 3. It was anticipated that such a metal plate short-circuited the polarization electric field in the beam and violated the undeflected propagation of the beam by the $\vec{E} \times \vec{B}$ drift.

(i) Relation of the electric field in the beam with the position of the metal plate

The electric field and the radial profile of the ion current density were measured under the situation where the metal plate was moved along $B_\perp$ field lines from $x = 2.5$ cm to $x = 12.5$ cm. (To set the metal plate in the region $4.0 \leq x \leq 12.5$ cm, it was cut to circle with the diameter of 9.5 cm.)

First, the metal plate was placed at $x = 2.5$ cm. In this arrangement, a part of beam ions was incident obliquely on the metal plate. Figure 16 shows the electric field strength E as a function of the $B_\perp$ strength in the range of 0 to 3 kG. The electric field strength is 1 kV/cm or less independent of the $B_\perp$ strength. This clearly shows that the electric field in the beam is shorted out by the metal plate. It made little difference to the electric field whether the metal plate was electrically isolated (the case in the present experiment) or grounded. In contrast to the electric field, the floating potential in the beam rose up from 4 kV to 9 kV with increasing the $B_\perp$ strength from 0.5 kG to 2 kG. Furthermore, this floating potential of 9 kV at $B_\perp = 2$ kG reduced to 2 kV when the metal plate was grounded with a low-inductance conductor. Profiles of the ion current and the net current densities in the y direction observed at $z = 6$ cm are shown in Fig. 17 for $B_\perp = 2$ kG. The peak of the ion current density is shifted to $y = 3$-4 cm, which almost agrees with $y = 4.6$ cm calculated from single-particle orbits of the ions under the Lorentz force (Section 5.E). The ion current density at the peak amounts to 10 A/cm^2. This value is about twice as much as 4.5 A/cm^2 observed at $B_\perp = 2$ kG in the case without the metal plate (Fig. 11), and is comparable to 11 A/cm^2 at $B_\perp = 0$. The net current density is nearly equal to the ion current density.

Second, the metal plate was placed at $x = 10$ cm, where the $B_\perp$ strength became maximum $[B_\perp(x = 10\text{ cm}) = 2.6B_\perp(x = 0)]$.

In this case, the electric field proportional to the $B_\perp$ strength was observed in the beam. Its value at $B_\perp = 2$ kG was 5.5-6.8 kV/cm, which was close to the theoretical value $E = \bar{u}_0 B_\perp = 7.2$ kV/cm. The profile of the ion current density observed at $z = 6$ cm for $B_\perp = 2$ kG is shown in Fig. 18, which fits with the one in the case without the metal plate (Fig. 11). This shows that the metal plate placed at $x = 10$ cm has no effect on the beam propagation across the magnetic field.

Finally, the relation between the electric field strength E and the position x of the metal plate was investigated over a range of x from 2.5 cm to 12.5 cm. The result for $B_\perp = 2$ kG is shown in Fig. 19. The electric field strength of 5.0-7.1 kV/cm close to the theoretical value $E = 7.2$ kV/cm is observed in the range $7 \leq x \leq 12.5$ cm. In the range $2.5 \leq x < 7$ cm, on the other hand, the electric field strength decreases rapidly to less than 1 kV/cm with decreasing x. Similar observations were also obtained at $B_\perp = 1$ kG (Fig. 19): The electric field strength increases gradually from 3.2 kV/cm to 3.8 kV/cm with increasing x in the range $5.0 \leq x \leq 12.5$ cm. These values of the electric field strength agree with the theoretical value $E = 3.6$ kV/cm at $B_\perp = 1$ kG. In the range $2.5 \leq x < 5$ cm, however, the electric field strength is 1 kV/cm or less. Here, it should be noted that the beam is expanded along $B_\perp$ field lines from $x = 3$-4 cm at $B_\perp = 0$ to $x = 6$-8 cm when $B_\perp = 2$ kG and no metal plate is placed in the magnetic field (Section 4.B.(i)).

Thus, the following conclusion can be derived from the above experimental results: The short circuit of the polarization electric field occurs only when the metal plate is placed so close as to come in contact with the beam; otherwise, the polarization electric field is retained in the beam and the beam crosses the magnetic field without deflection.

(ii) Axial distribution of the electric field near the entrance to the short-circuit region

The probes were fixed at $z = 0$ while the metal plate was made movable along the z axis on the plane $x = 2.5$ cm, as shown in Fig. 20. The electric field strength E in the beam was measured under the condition that the position z of the upstream edge of the metal plate was varied from -6 cm to 6 cm. This experiment was carried out at both $B_\perp = 1$ kG and $B_\perp = 2$ kG. The purpose of this experiment is to investigate the distribution in the z direction of the electric field strength near the entrance ($z = 0$) to the short-circuit region. The short-circuit region is defined as a region in the vacuum vessel where $B_\perp$ field lines which are intersected by the metal plate fill. Obtained data of the electric field strength were arranged and plotted as a function of the relative position z_r of the probes to the metal plate. It should be noted that $z_r = -z$. The results are shown in Fig. 21. The beam proceeds toward $+z_r$ in the figure. In the region $z_r \geq 0$, $B_\perp$ field lines are intersected by the metal plate at $x = 2.5$ cm and define the short-circuit region.

When $B_\perp = 1$ kG, the electric field strength of 3.4-4.2 kV/cm is observed independent of z_r in the region $-6 \leq z_r \leq -3$ cm. These values of the electric field strength agree with the theoretical prediction $E = \bar{u}_0 B_\perp = 3.6$ kV/cm. On the other hand, the electric field is short-circuited by the metal plate and its strength is decreased to 1 kV/cm or less in the region $2 \leq z_r \leq 6$ cm. Similar features are observed at $B_\perp = 2$ kG: The electric field strength reaches 5.7-6.9 kV/cm close to the theoretical value $E = 7.2$ kV/cm in the region $-6 \leq z_r \leq -1$ cm, while it decreases to 1.5 kV/cm or less in the region $1 \leq z_r \leq 6$ cm. These results clearly show that the short circuit of the electric field occurs only in the short-circuit region, that is, in the region $z_r \geq 0$.

A width Δz_r of the transition layer from $E \simeq \bar{u}_0 B_\perp$ to $E \simeq 0$ is about 4 cm at $B_\perp = 1$ kG and 1-2 cm at $B_\perp = 2$ kG. This means that Δz_r decreases with increasing the strength of $B_\perp$. The reason for this may be that Δz_r is related with gyro-motions of beam ions and electrons. Gyroradii ρ_i, ρ_e and $\rho_h = (\rho_i \rho_e)^{1/2}$ are evaluated from ion and electron velocities of 3.6×10^8 cm/s and $B_\perp = 1$ kG to be 36 cm, 0.02 cm and 0.8 cm, respectively. At $B_\perp = 2$ kG, all the above values of ρ_i, ρ_e and ρ_h are halved. It is not clear yet what determines Δz_r

5. DISCUSSION

A. Applicability of the steady-state model to the experiment

The model for beam propagation presented in Section 2 assumes the beam current injected into the magnetic field to be independent of time in order to derive the steady-state solutions. This assumption, however, appears not to be satisfied in the present experiment because the beam current varies with time in the experiment.

First, we introduce T_p; the scale time for the beam to complete the polarization and T_b; the scale time of variation in the beam current. We next imagine that the beam is divided into elements at every time-width T_p. Then, the beam current can be regarded to be constant with respect to time in each element of the beam and the steady-state model for beam propagation applys to each element of the beam if the condition $T_p << T_b$ is satisfied. The complete solution to the whole of the beam is given as the summation of the solution to each element of the beam. In other words, the quasi-steady state of the polarization is established in the whole of the beam if the condition $T_p << T_b$ is satisfied, and the steady-state model for beam propagation can be applied to this beam. The time T_p is given from eqs. (12)-(14) as $\rho_h/\sqrt{\kappa}u_0$, which reduces to ω_e^{-1} for $\kappa >> 1$. Scale times T_p and T_b are evaluated (for the main part of the beam) to be $T_p = \omega_e^{-1} \lesssim 1$ ns and $T_b \sim 100$ ns from data of the present experiment. The condition $T_p << T_b$ holds well so that the model presented in Section 2 can be applied to the present experiment.

B. Condition of the beam thickness for the propagation

Here, we check whether our experimental data meet the criterion for the beam thickness w, $\rho_i/\kappa << w < \rho_i/2$ derived from eqs. (18) and (19). In the experiment at the $B_\perp$ strength of up to 3 kG, the beam thickness w was 4.0-4.5 cm at the middle (z = 0) of the $B_\perp$ region independent of the $B_\perp$ strength. Values of κ at z = 0 were 2300 ($B_\perp$ = 1 kG), 500 ($B_\perp$ = 2 kG) and 140 ($B_\perp$ = 3 kG). The ion gyroradius can be evaluated from the beam velocity of 3.6×10^8 cm/s and the $B_\perp$ strength. Using these numerical values, we can express the criterion as 0.016 cm $<<$ w $<$ 18 cm ($B_\perp$ = 1 kG), 0.036 cm $<<$ w $<$ 9 cm ($B_\perp$ = 2 kG) and 0.086 cm $<<$ w $<$ 6 cm ($B_\perp$ = 3 kG). Thus, it is clear that the beam meets the criterion in this range of the $B_\perp$ strength.

C. Condition of κ required for the beam propagation

In the simplified model presented in Section 2, the requirement for the undeflected propagation of the beam across the magnetic field was $\kappa >> 1$. Recently, Peter and

Rostoker[33)] derived analytically the stronger condition $\kappa \gg (m_i/m_e)^{1/2}$ to be satisfied from the requirement of the longitudinal quasi-neutrality of the beam in the course of propagation. The validity of this condition, however, has never been confirmed by experiment. Here, (i) we follow their theory briefly. Then, (ii) we present an empirical relation between the electric field strength in the beam and κ, which gives the lower bound of κ necessary for the formation of the polarization electric field. The relation is compared with the above theory.

(i) Theory

The validity of quasi-neutrality assumption ($n_i = n_e$) is checked by solving for the perturbation in charge density $\delta n/n_0$. From Poisson's equation, the space charge density is related with E_z as

$$\frac{n_i - n_e}{n_0} = \frac{\varepsilon_0}{en_0}\frac{\partial}{\partial z}E_z .$$

From the relation $E_z = v\,B_\perp$ and eq. (7), this expression becomes

$$\frac{n_i - n_e}{n_0} = \frac{\Omega_i\Omega_e}{\omega_i^2}\left(1 + \frac{E_y/B_\perp}{u}\right),$$

where E_y can be written in the form (Appendix A)

$$E_y = -u_0 B_\perp (\omega_i^2/\Omega_i^2)(u_0 - u)/u. \tag{24}$$

Using eq. (24) and the relation $\kappa = 1 + \omega_i^2/\Omega_i^2$, we obtain

$$\frac{n_i - n_e}{n_0} = \frac{m_i}{m_e}\left[\frac{1}{\kappa - 1} - \frac{u_0(u_0 - u)}{u^2}\right].$$

When the term $u_0(u_0 - u)/u^2$ is evaluated from eq. (12) to order κ^{-1}, this expression yields

$$\frac{n_i - n_e}{n_0} = \frac{m_i}{m_e}\left[\frac{1}{\kappa - 1} - \frac{1}{\kappa}\left(1 - \cos\frac{\sqrt{\kappa} z}{\rho_h}\right)\right].$$

After averaging out the spacial oscillations, we obtain

$$\frac{\delta n}{n_0} = \frac{\bar{n}_i - \bar{n}_e}{n_0} = \frac{m_i}{m_e}\frac{1}{\kappa(\kappa - 1)} .$$

The quasi-neutrality condition $\delta n/n_0 \ll 1$ then requires

$$\kappa \gg (m_i/m_e)^{1/2}. \tag{25}$$

(ii)Experiment

Figure 15 shows that the number density (or equivalently the value of κ) of the beam is large enough to establish the full electric field strength $E = \bar{u}_0 B_\perp$ by the polarization in the region $-4.5 \le x \le 4.5$ cm but it is not large enough in the region $x > 4.5$ cm. Therefore, we can determine the condition of κ necessary for the formation of the polarization electric field by investigating the relation of the normalized electric field strength $E/\bar{u}_0 B_\perp$ with κ. This relation, for example, in the case of $B_\perp = 1$ kG is derived as follows: The distribution of $E/\bar{u}_0 B_\perp$ on the x axis is calculated from the distribution of the electric field strength E on the x axis shown in Fig. 15, the profile of $B_\perp$ on the x axis for $B_\perp = 1$ kG and $\bar{u}_0 = 3.6 \times 10^8$ cm/s. The dielectric constant κ is expressed in terms of the ion current density J_i, $\bar{u}_0$ and $B_\perp$ as

$$\kappa = 1 + \frac{m_i J_i}{\varepsilon_0 e \bar{u}_0 B_\perp^2} . \tag{26}$$

We can therefore obtain the distribution of κ on the x axis, using eq. (26), from profiles of J_i and $B_\perp$ on the x axis ($B_\perp = 1$ kG) and $\bar{u}_0 = 3.6 \times 10^8$ cm/s. Correspondence between these distributions of $E/\bar{u}_0 B_\perp$ and κ at every x yields directly the relation of $E/\bar{u}_0 B_\perp$ with κ at $B_\perp = 1$ kG. The same procedure is also taken at $B_\perp = 2$ kG. The results are shown in Fig. 22 with closed circles ($B_\perp = 1$ kG) and open circles ($B_\perp = 2$ kG).

The value of κ changes over a range 20-2000. In the range $100 \leq \kappa \leq 2000$, $E/\bar{u}_0 B_\perp$ is almost unity independent of κ, while $E/\bar{u}_0 B_\perp$ reduces from unity to 0.2 in the range $20 \leq \kappa < 100$. As a result, the condition of κ required for the formation of the polarization electric field is found to be $\kappa \geq 100$, which is also consistent with the theoretical prediction $\kappa \gg (m_i/m_e)^{1/2} = 43$ for protons. In Fig. 14, the electric field strength E in the beam was shown to satisfy the theoretical relation $E = \bar{u}_0 B_\perp$ at the $B_\perp$ strength of up to 3 kG. This result is also reasonable from the above conclusion because the value of κ was always larger than 140 in this range of the $B_\perp$ strength.

D. Short circuit of the polarization electric field by means of a metal plate

It was concluded in Section 4.C.(i) that the short circuit of the polarization electric field occured only when the beam was in contact with the metal plate. A qualitative interpretation for this conclusion is presented below.

The short circuit of the polarization electric field is caused by the electron flow along $B_\perp$ field lines from the negative charge layer into the positive charge layer through the metal plate. First, let us suppose that the metal plate is located far from the beam. The x component of the polarization electric field, E_x accelerates electrons in the negative charge layer toward the metal plate along $B_\perp$ field lines. When the electrons leave the negative charge layer in this situation, the positive charge left behind will produce a space-charge field much larger than E_x and pull the electrons back before they reach the metal plate. Even if the electrons reached the metal plate, they could not flow into the positive charge layer because a strong electric field (much stronger than E_x on the metal plate) would be necessary to extract the electrons from the metal plate by field emission.

Next, let us suppose that the beam is in contact with the metal plate. In this case, a part of beam ions is expected to bombard the surface of the metal plate and produce electrons on the metal plate by secondary emission instead of field emission, as discussed later. When the electrons in the negative charge layer are accelerated to the metal plate, the secondary electrons on the metal plate will flow into the positive charge layer in the same manner. The beam as a whole remains space-charge-neutral, so that the electrons can easily flow from the negative charge layer into the positive charge layer.

A possibility that secondary emission by ion bombardment is the mechanism for the production of neutralizing electrons on the metal plate, is examined below. The secondary electron yield γ is expressed by the equation[36)]

$$\gamma(\theta) = \gamma_0 \sec(\theta), \tag{27}$$

where γ_0 is the yield at normal incidence and θ is the incident angle. For a 70 keV ion (proton) incident on the flat surface of stainless steel (SUS 304), the yield γ_0 is $\simeq 5$. The angle θ is considered to be of the order of $90° - 4°$ where 4° is the half divergence angle of the beam. When these values are substituted to eq. (27), we obtain $\gamma \simeq 10^2$. Therefore, $\gtrsim 10^{-2}N$ ions (N: the total number of ions in the beam) have to bombard the metal plate to produce secondary electrons sufficient for the space-charge neutralization, while it is found from calculation that $\gtrsim 5 \times 10^{-2}N$ ions are incident on the metal plate when the metal plate is placed in the region $x \lesssim 2.5$ cm.

E. Effects of a metal plate on the beam propagation

Characteristic behaviors of the beam observed when the polarization electric field is short-circuited are presented in Fig. 17 and are summarized to the following three points:

1) The net current density is nearly equal to the ion current density, that is, the current neutrality of the beam is broken.
2) The peak value of the ion current density amounts to 10 A/cm^2, which is about twice as much as 4.5 A/cm^2 observed when $B_\perp$ = 2 kG and no metal plate is placed.
3) The shift of the current peak to y = 3-4 cm agrees with y = 4.6 cm calculated from single-particle orbits of beam ions.

Here, the shift y was calculated from the following simplified model: An ion beam with a velocity of 3.6×10^8 cm/s undergoes only the Lorentz force over a distance l = 12 cm from z = -6 cm to z = 6 cm (l: the width of the metal plate). The strength of $B_\perp$ is treated as constant in this region. Then, y is expressed as

$$y = \rho_i - (\rho_i^2 - 1^2)^{1/2}. \quad (28)$$

When ρ_i = 18 cm at $B_\perp$ = 2 kG is substituted to eq. (28), we obtain y = 4.6 cm.

Observation 1) shows that motions of the electrons across $B_\perp$ are impossible without the aid of the polarization electric field. Gyroradii of the electrons ($\sim 10^{-2}$ cm) are much smaller than those of the ions (≃ 18 cm) in the magnetic field (2 kG), so that the electrons are tied to $B_\perp$ field lines at the entrance to the short-circuit region and stop, while the ions penetrate further into the magnetic field, subjected to deflections by the Lorentz force.

One of the reasons for observation 2) is that the expansion of the beam along $B_\perp$ field lines and the resultant decrease in the ion current density are prevented by the short circuit of the polarization electric field. The other reason is that as the ion space charge is almost completely neutralized by electrons (from the metal plate), blowup of the beam caused by strong space-charge fields is prevented.

When the space-charge neutralization of the beam is accomplished, observation 3) is reasonable since the kinetic pressure $m_i n u^2/2$ of the beam is about an order of magnitude less than the pressure $B_\perp^2/2\mu_0$ of the magnetic field $B_\perp$ so that the undeflected propagation of the beam across the magnetic field due to the diamagnetic effect is unlikely.

CONCLUSION

The propagation of the intense neutralized ion beam as a low-beta, large-gyroradius plasma stream across the magnetic field was studied experimentally under conditions both without and with the metal plate in the magnetic field. The space-charge-neutralized and current-neutralized beam of protons was produced by the reflex triode and injected into the transverse magnetic field $B_\perp$ of up to 3 kG. The beam has the following parameters: the average velocity $\bar{u}_0$ of 3.6×10^8 cm/s, the velocity spread of 0.9×10^8 cm/s, the ion current density of 18 A/cm^2 and the duration of 200-300 ns. It was observed that the beam propagated across the magnetic field without deflection. Main results derived from the present study are as follows:

1) The polarization electric field E_y was observed in the beam, which agreed with the theoretical relation $E_y = -\bar{u}_0 B_\perp$ for the beam with the velocity spread. The mechanism of the cross-field propagation was, therefore, identified to be the $\vec{E} \times \vec{B}$ drift due to the polarization electric field E_y.
2) When the strength of the magnetic field varied spacially in the beam, the polarization electric field satisfied the relation $E_y = -\bar{u}_0 B_\perp$ locally in accordance with the spacial variation in the magnetic field strength.
3) The condition of the dielectric constant κ for the formation of the polarization electric field $E_y = -\bar{u}_0 B_\perp$

was derived from the present experiment to be $\kappa \geq 100$. This condition was consistent with the theoretical prediction $\kappa \gg (m_i/m_e)^{1/2} = 43$.

4) The polarization electric field was short-circuited by the metal plate only when the plate was placed in the magnetic field so as to come in contact with the beam; then, the beam was deflected according to single-particle orbits of beam ions under the Lorentz force.

As a result, the present study has proved that the intense neutralized ion beam as a low-beta, large-gyroradius plasma stream propagates across the magnetic field by means of the $\vec{E} \times \vec{B}$ drift due to the polarization electric field when the condition $\kappa \geq 100$ is satisfied.

ACKNOWLEDGEMENT

The author would like to thank Professor T. Kawabe for his continuing guidance and encouragement through this work. The author is indebted to Professor S. Miyoshi for his interest and guidance. The author acknowledges the helpful discussion with Professor H. Ishizuka and Dr. K. Kamada. The author also thanks Professor K. Sawada, Professor K. Yatsu, Professor M. Inutake, Professor Y. Kiwamoto, Professor A. Mase, Dr. A. Itakura, Dr. K. Ishii, Dr. I. Katanuma, Dr. T. Saito and the members of plasma group of the University of Tsukuba for their helpful advice.

APPENDIX A

A steady-state model for the beam propagation by Sinelnikov and Rutkevich

In the steady state, differentiation with respect to time can be transformed into differentiation with respect to z:

$$\frac{d}{dt} = \frac{\partial}{\partial t} + \frac{dz}{dt}\frac{\partial}{\partial z} = u\frac{d}{dz} .$$

Then, the model equations (3) and (4) are written as

$$u_i \frac{d}{dz} v_i = \frac{e}{m_i}(E_y + u_i B_\perp) + \frac{m_e}{m_i}\nu(v_e - v_i), \tag{A1}$$

$$u_i \frac{d}{dz} u_i = \frac{e}{m_i}(E_z - v_i B_\perp) + \frac{m_e}{m_i}\nu(u_e - u_i), \tag{A2}$$

$$u_e \frac{d}{dz} v_e = -\frac{e}{m_e}(E_y + u_e B_\perp) - \nu(v_e - v_i), \tag{A3}$$

$$u_e \frac{d}{dz} u_e = -\frac{e}{m_e}(E_z - v_e B_\perp) - \nu(u_e - u_i). \tag{A4}$$

From eqs. (5) and (6), it follows that

$$\frac{d}{dz}(n_i u_i) = 0,$$

$$\frac{d}{dz}(n_e u_e) = 0,$$

and eventually

$$n_i u_i = n_e u_e = n_0 u_0 . \qquad \text{(A5)}$$

We assume that the beam is so dense as to remain quasi-neutral ($n_i = n_e = n$) in the magnetic field. This assumption comes from the following consideration: Let us consider forces acting on ions and electrons of the beam in the direction of the beam propagation (the z direction). The Lorentz force F_M acts so as to separate ions and electrons to each other in the z direction and to break the quasi-neutrality of the beam because of the large difference in gyroradius between ions and electrons. The charge separation of ions and electrons now causes an electric force $F_E = qE_z$ which acts so as to restore the quasi-neutrality of the beam. Forces F_M and F_E have maximum values of $qu_0B_\perp$ and $q^2n_0\rho_i/\varepsilon_0$, respectively. The ratio of F_M to F_E is then expressed as

$$\frac{F_M}{F_E} \simeq \frac{1}{\kappa} \propto \frac{1}{n_0} .$$

Therefore, if the initial density n_0 of the beam is large enough to be $\kappa >> 1$, the electric force F_E will overcome the Lorentz force F_M and the quasi-neutrality of the beam will be retained. This consideration is very rough and the validity of the quasi-neutrality assumption must be checked more exactly. (The validity of this assumption is discussed in Section 5.C.) Combined with the continuity of the ion and electron currents expressed by eq. (A5), this assumption yields

$$u_i = u_e = u = u_0(n_0/n). \tag{A6}$$

Equations (A1)-(A6) can be expressed in terms of the relative velocity $v = v_i - v_e$ and u as

$$u\frac{dv}{dz} + \nu v = \frac{e}{m_e}E_y + \Omega_e u, \tag{A7}$$

$$u\frac{du}{dz} = -\Omega_i v, \tag{A8}$$

where terms of order $m_e/m_i << 1$ are omitted. Note that E_z is missed in eqs. (A7) and (A8) because of eq. (A6). The transverse polarization field E_y is taken in the form

$$E_y = -\frac{en}{\varepsilon_0}\delta y = -\frac{en_0u_0}{\varepsilon_0 u}\delta y, \tag{A9}$$

where $\delta y = y_i - y_e$. Equation (A8) is integrated with the aid of the relation

$$v = \frac{d}{dt}\delta y = u\frac{d}{dz}\delta y,$$

and we have

$$\delta y = \frac{u_0 - u}{\Omega_i} . \tag{A10}$$

From eqs. (A7)-(A10), we obtain the following set of equations:

$$\frac{dv}{dz} + \nu\frac{v}{u} = -\frac{\omega_e^2}{\Omega_e}\frac{u_0(u_0 - u)}{u^2} + \Omega_e, \tag{A11}$$

$$\frac{du}{dz} = -\Omega_i\frac{v}{u}, \tag{A12}$$

where $\omega_e = (e^2 n_0/m_e\varepsilon_0)^{1/2}$ is the electron plasma frequency. Equations (A11) and (A12) can be solved for $\xi = 1 - u/u_0 << 1$. The results are

$$\xi = \frac{1}{\kappa}[1 - (\cos\gamma z + \frac{\nu}{2u_0\gamma}\sin\gamma z)\exp(-\frac{\nu z}{2u_0})], \tag{A13}$$

$$\gamma = \frac{1}{u_0}(\omega^{*2} - \frac{\nu^2}{4})^{1/2}, \tag{A14}$$

where $\omega^* = (\kappa\Omega_e\Omega_i)^{1/2}$ is equal to ω_e for $\kappa >> 1$. It is found from eq. (A13) that the assumption $\xi << 1$ is valid if the condition $\kappa >> 1$ is satisfied. From eqs. (A13) and (A14), we can derive the beam velocity u, the relative displacement δy and the polarization electric field E_y to order κ^{-1}. The results for limiting cases of 1) $0 < \nu << 2\omega^*$, 2) $\nu = 2\omega^*$ and 3) $\nu >> 2\omega^*$ are given below and are also illustrated in Figs. A1, A2 and A3, respectively.

1) $0 < \nu << 2\omega^*$

$$u = u_0[1 - \frac{1}{\kappa}[1 - \exp(-\frac{\nu z}{2u_0})\cos\frac{\sqrt{\kappa}z}{\rho_h}]], \tag{A15}$$

$$\delta y = \frac{\rho_i}{\kappa}[1 - \exp(-\frac{\nu z}{2u_0})\cos\frac{\sqrt{\kappa}z}{\rho_h}], \tag{A16}$$

$$E_y = -u_0 B_\perp [1 - \exp(-\frac{\nu z}{2u_0})\cos\frac{\sqrt{\kappa}z}{\rho_h}]$$

$$\times[1 - \frac{1}{\kappa}\exp(-\frac{\nu z}{2u_0})\cos\frac{\sqrt{\kappa}z}{\rho_h}], \tag{A17}$$

Equations (A15)-(A17) have the form of damped oscillations. For $z >> 2u_0/\nu >> \rho_h \kappa^{-1/2}$, we obtain

$$u = u_0(1 - \frac{1}{\kappa}), \tag{A18}$$

$$\delta y = \frac{\rho_i}{\kappa}, \tag{A19}$$

$$E_y = -u_0 B_\perp . \tag{A20}$$

2) $\nu = 2\omega^*$

$$u = u_0[1 - \frac{1}{\kappa}[1 - (1 + \frac{\nu z}{2u_0})\exp(-\frac{\nu z}{2u_0})]], \tag{A21}$$

$$\delta y = \frac{\rho_i}{\kappa}[1 - (1 + \frac{\nu z}{2u_0})\exp(-\frac{\nu z}{2u_0})], \tag{A22}$$

$$E_y = -u_0 B_\perp [1 - (1 + \frac{\nu z}{2u_0})\exp(-\frac{\nu z}{2u_0})]$$

$$\times[1 + \frac{1}{\kappa}(1 + \frac{\nu z}{2u_0})\exp(-\frac{\nu z}{2u_0})]. \tag{A23}$$

Oscillatory behaviors of u, δy and E_y are not seen in eqs. (A21)-(A23) because of the damping of oscillations due to effective collisions between ions and electrons. For $z >> 2u_o/\nu = \rho_h \kappa^{-1/2}$, eqs. (A21)-(A23) reduce to eqs. (A18)-(A20), respectively.

3) $\nu >> 2\omega^*$

$$u = u_0 [1 - \frac{1}{\kappa}[1 - \exp(-\frac{\nu z}{u_0})]], \tag{A24}$$

$$\delta y = \frac{\rho_i}{\kappa}[1 - \exp(-\frac{\nu z}{u_0})], \tag{A25}$$

$$E_y = -u_0 B_\perp [1 - \exp(-\frac{\nu z}{u_0})][1 - \frac{1}{\kappa}\exp(-\frac{\nu z}{u_0})]. \tag{A26}$$

Equations (A24)-(A26) also reduce to eqs. (A18)-(A20), respectively in the shorter distance $z \sim \rho_h \kappa^{-1/2} >> u_0/\nu$ because of the strong damping.

APPENDIX B

Characteristics of the reflex triode

B1. The mechanism of ion beam production in the reflex triode

We describe the operation of the reflex triode as the source of intense neutralized ion beams. Suppose that an anode made of a thin, plastic foil and a cathode at ground potential are faced to each other. Immediately after the application of a positive high voltage to the anode with respect to the cathode, electrons are emitted from the cathode by field emission and are accelerated toward the anode. Most of electrons pass through the anode and proceed to the opposite side. Electrons which passed through the anode are then decelerated due to their own space-charge and are reflected back toward the anode. This location in vacuum where electrons are reflected is called a virtual cathode because the potential at the turning point of electrons becomes equal to that at the cathode. Thus, electrons repeat multiple reflections between the cathode and the virtual cathode through the anode until they are finally absorbed in the anode losing their kinetic energy. During these motions of electrons, a dense plasma is formed on the anode. (We refer to this plasma as an anode plasma.) Ions in the anode plasma are then accelerated to both sides and form ion beams. The mechanism of the anode plasma formation has never been identified. Surface flashover of the anode due to a tangential component of the electric field, however, has been proposed to be most probable. The efficiency of ion beam production $I_i/(I_i + I_e)$ under the existence of multiple reflections of electrons is roughly calculated as

$$\frac{I_i}{I_i + I_e} = [1 + \frac{(m_i/m_e)^{1/2}}{2\eta + 1}]^{-1}, \tag{B1}$$

where η is the number of transit through the anode by a single electron. Since the ion beam is extracted only in the virtual-cathode side, the practical efficiency becomes a half of eq. (B1). Equation (B1) shows that the efficiency increases with increasing η. In the present experiment, the anode voltage of 70 kV and the Mylar anode with the thickness of 4 μm give $\eta \simeq 3$. Therefore, the efficiency expected from eq. (B1) is 7 %. On the other hand, the efficiency derived from the experiment is about 4 %. The origin of this disagreement by a factor of 2 is not clear. It should be, however, taken into account that the physical model for eq. (B1) assumes $\eta >> 1$ implicitly but this condition is not satisfied in the present experiment.

The ion beam emerging from the triode captures electrons at the virtual cathode and becomes space-charge-neutral and current-neutral. This enables for the beam to propagate in free space without spreading out due to the space-charge repulsion among beam ions. Mechanisms of the space-charge neutralization and the current neutralization are not fully understood though they have been studied by many authors.[B1,B2)

In the initial phase before the anode plasma is formed, the diode current is carried by only the electron flow and in general is very small due to the space-charge limit in the axial direction. This phase is called a high impedance phase. The space charge of electrons also produces a radial electric field which causes outward drifts of electrons and increases their loss to the anode support. In the actual operation of the reflex triode, an axial magnetic field B_z is applied to the triode to suppress the drifts of electrons. After a dense plasma is formed on the anode, the space charge of electrons is completely neutralized by ions emitted from the plasma. The diode current is then carried by the ion and electron flows and increases rapidly. This phase accompanied by the emission of ions is called an ion flow mode. In the period of the ion flow mode, the diode current produces an azimuthal magnetic field B_θ of the considerable strength, which distorts orbits of reflexing electrons in the radial direction. This leads to the loss of electrons to the anode support and as a result, to the reduction in the efficiency of ion beam production. The axial magnetic field B_z plays again a role of eliminating the effect of the B_θ field if the B_z field is strong enough to be $B_z >> B_\theta$.

B2. Formation of the anode plasma

Time-resolved pictures of the light from the anode plasma were taken by means of a framing camera to investigate the formation and the time evolution of the anode plasma. Obtained pictures were related with waveforms of the anode voltage and the diode current. Figure B1(a) shows framing pictures taken from the side of the reflex triode. The field of view of the camera is shown in Fig. B1(b). The timing of each framing picture is indicated with figures [1]-[8] on the waveform of the anode voltage in Fig. B1(c). The formation of the anode plasma initiates at the end of the first plateau of the anode voltage (namely, at the end of the high impedance phase) as shown in the picture [1]. The anode plasma covers all over the surface of the anode in 50-100 ns (pictures [2] and [3]). In this period, the anode voltage drops to the second plateau of 100 kV (ion flow mode) where the emission of beam ions occurs. The drop in the anode voltage is attributed to a serial inductance L of the Marx generator and the triode circuit, which causes an inductive drop $L\dot{I}$ of about 100 kV when the diode current increases rapidly. The ion flow mode terminates in 200-250 ns, accompanied by the decay in the anode voltage to zero. The cause of the termination of the ion flow mode is the short circuit between the anode and the cathode pin by the anode plasma expanding toward the cathode as shown in pictures [7] and [8]. The expansion of the anode plasma is

not uniform within the diameter of the anode but it is marked in front of the cathode pin where the expansion velocity of the plasma is evaluated to be 2.5×10^6 cm/s from the pictures in Fig. B1(a). A qurious phenomenon which is not interpreted yet is a high-frequency vibration of the cathode pin appearing in pictures [4]-[6]. The vibration of the cathode pin appears only in the period while the production and the acceleration of beam ions occur. The frequency of vibration can be estimated to be more than 50 MHz.
Figure B2(a) shows framing pictures taken from the front of the triode. Figure B2(b) and (c) indicates the field of view of the camera and the timing of each framing picture respectively, as in Fig. B1. At first, the plasma is produced in the form of a spot on the anode just in front of the cathode pin (the picture [2]). The plasma then expands in the radial direction and finally covers the whole surface of the anode in a time less than 100 ns.

Next, we removed the cathode pin in order to investigate the effect of the cathode pin on the formation of the anode plasma. Framing pictures of the anode plasma were taken from the front of the triode. The result for a typical shot is shown in Fig. B3. In this case, the start of the plasma formation is delayed compared with the case with the cathode pin. The delay time is not fixed but varies shot by shot within about 100 ns. The duration of the high impedance phase is increased as much. Furthermore, the plasma is produced shot by shot at irregular locations on the anode in front of the edge of the cathode (the picture [3]). Poor reproducibilities of the anode voltage and the beam current observed under the condition of no cathode pin are attributable to these temporal and spacial irregularities in the formation of the anode plasma.

B3. Effects of an axial magnetic field B_z on the operation of the reflex triode

The strength of the axial magnetic field B_z affects on the anode voltage, the diode current and the beam current. Figure B4 shows waveforms of the anode voltage and the diode current for different values of B_z. The beam current which is detected at 37 cm downstream from the anode ($z = -13$ cm) on the z axis is shown as a function of the strength of B_z in Fig. B5. When no B_z is applied, the anode voltage of 180-230 kV lasts for 400 ns in the high impedance phase and subsequently it drops to zero without staying in the ion flow mode (Fig. B4(a)). Then, the beam current is not detected (Fig. B5). As the strength of B_z increases, the duration of the high impedance phase and the anode voltage in this phase decrease. The second plateau region in the anode voltage, that is, the ion flow mode appears at $B_z = 4$ kG; then, the diode current rises rapidly at the beginning of the ion flow mode (Fig. B4(c)). The beam current detected at $B_z = 4$ kG amounts to about five times as much as that at $B_z = 2$ kG (Fig. B5). At the B_z field of more than 4 kG, waveforms of the anode voltage and the diode current are not changed from those at B_z = 4 kG (Fig. B4(c), (d) and (e)); however, the beam current increases gradually with increasing B_z (Fig. B5).

These results derived from Figs. B4 and B5 can be interpreted as follows: In the case of $B_z = 0$, most of electrons emitted from the cathode diverse due to their own space-charge in the radial direction and are lost to the anode support. The loss of electrons makes the prompt formation of the anode plasma difficult and results in the longer duration of the high impedance phase. The azimuthal magnetic field B_θ produced by the diode current I at the radius r_c of the cathode is given by

$$B_\theta = \frac{\mu_0}{2\pi} \frac{I}{r_c} .$$

For our typical case of I = 10 kA and r_c = 1.25 cm, B_θ becomes 1.6 kG. When the B_z field is weaker than the B_θ field of 1.6 kG, it is anticipated that the B_θ field gives serious disturbances on one-dimensional reflexing motions of electrons and decreases the number of electron transit through the anode. As a result, this causes the collapse of the ion flow mode and leads to the poor efficiency of the ion beam production. When the B_z field is sufficiently stronger than the B_θ field of 1.6 kG, on the other hand, the one-dimensionality of the electron motion is assured by the B_z field and the B_θ field does not have an appreciable effect on the characteristics of the reflex triode. The experimental result shown in Fig. B5, that is, the rapid increase in the beam current between B_z = 2 kG and B_z = 4 kG is reasonable from the above consideration.

In summary, Framing pictures of the light from the anode plasma are well correlated with waveforms of the anode voltage and the diode current and give some informations on the time evolution of the anode plasma. A pin set on the cathode plays a role of triggering the discharge and allows the prompt and reproducible formation of the anode plasma. The axial magnetic field B_z which is sufficiently stronger than the azimuthal magnetic field B_θ produced by the diode current, must be applied to the triode to assure the efficient production of the ion beam.

REFERENCES

1) D. M. Westone, M. P. Ehrlich and D. Finkelstein: Phys. Fluids 3(1960)617.

2) E. H. Beckner: Phys. Fluids 7(1964)586.

3) D. A. Baker and J. E. Hammel: Phys. Fluids 8(1965)713.

4) R. A. Dory, D. W. Kerst, D. M. Meade, W. E. Wilson and C. W. Erickson: Phys. Fluids 9(1966)997.

5) G. O. Barney: Phys. Fluids 12(1969)2429.

6) J. L. Tuck: Phys. Rev. Lett. 3(1959)313.

7) P. D. Markovic and F. R. Scott: Phys. Fluids 14(1971)1742.

8) C. E. Speck, J. J. Lee and O. K. Mawardi: IEEE Trans. Plasma Sci. 5(1977)151.

9) L. Lindberg and L. Kristoferson: Cosmic Electrodynamics 2(1971)305.

10) Y. Tanaka, K. Ohya, T. Okuda and K. Yamamoto: J. Phys. Soc. Jpn. 32 (1972)510.

11) A. Komori, N. Sato, H. Sugai and Y. Hatta: Plasma Phys. 19(1977)283.

12) G. Schmidt: Phys. Fluids 3(1960)961.

13) F. F. Chen: Introduction to Plasma Physics (Plenum Press, 1974) P. 39.

14) S. Humphries, Jr.: Nucl. Fusion 20(1980)1549.

15) S. Humphries, Jr., J. J. Lee and R. N. Sudan: Appl. Phys. Lett. 25(1974)20.

16) G. Cooperstein, S. A. Goldstein, D. Mosher, F. W. Oliphant, F. L. Sandel, S. J. Stephanakis and F. C. Young:

Proceedings of the 3 rd International Topical Conference on High Power Electron and Ion Beam Reseach and Technology. Novosibirsk July, 1979.

17) N. Ninomiya, M. Den, N. Nakamura and I. Minai: Kakuyugokenkyu, 41 Bessatsu 1(1979)7.

18) D. S. Prono, J. W. Shearer and R. J. Briggs: Phys. Rev. Lett. 37(1976)21.

19) S. Humphries, Jr., C. Eichenberger and R. N. Sudan: J. Appl. Phys. 48(1977)2738.

20) J. W. Poukey: Appl. Phys. Lett. 26(1975)145.

21) M. J. Clauser: Phys. Rev. Lett. 29(1975)145.

22) J. Shearer: Nucl. Fusion 15(1975)952.

23) H. H. Fleishmann and T. Kammash: Nucl. Fusion 15(1975)1143.

24) C. A. Kapetanakos, J. Golden, J. A. Pasour, S. J. Marsh and R. A. Mahaffey: Phys. Rev. Lett. 44(1980)1218.

25) R. V. Lovelace: Phys. Fluids 22(1979)542.

26) E. Otto and W. M. Manheimer: Nucl. Fusion 17(1977)1057.

27) W. M. Manheimer and N. K. Winsor: Nucl. Fusion 21(1981) 1559.

28) T. Ikehata, K. Kamada, H. Ishizuka, T. Kawabe and S. Miyoshi: Jpn. J. Appl. Phys. 21(1982)L186.

29) T. Ikehata, K. Kamada, H. Ishizuka, T. Kawabe and S. Miyoshi: Phys. Rev. A 25(1982)3415.

30) K. Kamada, C. Okada, T. Ikehata, H. Ishizuka and S. Miyoshi: J. Phys. Soc. Jpn. 46(1979)1963.

31) K. Kamada, C. Okada, T. Ikehata, H. Ishizuka and S. Miyoshi: J. Phys. Soc. Jpn. 51(1982)1290.

32) K. D. Sinelnikov and B. N. Rutkevich: Sov. Phys. Tech. Phys. 12(1967)37.

33) W. Peter and N. Rostoker: Phys. Fluids 25(1982)730.

34) In the experiment of ref. 3, the potential difference of more than 4 kV is observed in the direction transverse to the stream by cross-field injection of a plasma stream with an energy of 900 eV into the magnetic field of 6.5 kG. This result is inconsistent with the criterion of eq. (19).

35) W. Peter: Ph. D. dissertation, University of California, Irvine (1981).

36) K. Ohya and I. Mori: Jpn. J. Appl. Phys. 19(1980)L281.

B1) S. Humphries, Jr.: Appl. Phys. Lett. 32(1978)792.

B2) S. Humphries, Jr., T. R. Rockner, J. W. Poukey and J. P. Quintenz: Phys. Rev. Lett. 46(1981)995.

FIGURE CAPTIONS

Fig. 1	A simplified model of the cross-field propagation of an intense neutralized ion beam.
Fig. 2	Plots of u/u_0, $\delta y/\rho_i$ and $E_y/u_0 B_\perp$ from eqs. (10)-(12) versus distance $z/(\rho_i \rho_e)^{1/2}$ into the magnetic field. The value of κ is chosen to 100 (solid line) and 200 (dashed line).
Fig. 3	Schematic diagram of the experimental apparatus; (a) Marx generator, (b) anode, (c) cathode, (d) aperture, (e) voltage monitor, (f) charge collector, (g) a pair of Langmuir probes, (h) B_z coils, (i) $B_\perp$ coils and (j) Pyrex tube.
Fig. 4	Profiles of the strength of transverse magnetic field $B_\perp$.
Fig. 5	Schematic of Langmuir probe for the measurement of the polarization electric field.
Fig. 6	Schematic of charge collector.
Fig. 7	Typical oscillograms of anode voltage V and diode current I.
Fig. 8	Radial profiles of ion current density observed at $z = 0$ for $B_\perp = 0$.
Fig. 9	Velocity distribution function of beam ions (protons).
Fig.10	Radial profiles of ion current density observed at $z = 0$ for $B_\perp = 2$ kG.
Fig.11	Radial profiles of ion current density observed at $z = 6$ cm for $B_\perp = 2$ kG.

Fig.12 Physical process of the expansion of the beam along $B_\perp$ field lines.

Fig.13 Typical oscillograms of electric field E_y in the beam ([1] $B_\perp = 0$, [2] $B_\perp = 1$ kG, [3] $B_\perp = 2$ kG and [4] $B_\perp = 1$ kG in the opposite direction) and ion current.

Fig.14 Electric field strength E as a function of $B_\perp$ strength. The solid line represents the theoretical relation $E = \bar{u}_0 B_\perp$. Each point corresponds to the result of a single shot. Circles (triangles) are data points for $B_\perp$ in the + (-) x direction.

Fig.15 Distribution of electric field strength E on the x axis for $B_\perp = 1$ kG (closed circles) and $B_\perp = 2$ kG (open circles). Solid lines are from $E = \bar{u}_0 B_\perp$.

Fig.16 Electric field strength E as a function of $B_\perp$ strength in the case with a metal plate at $x = 2.5$ cm. Circles (triangles) are data points for $B_\perp$ in the + (-) x direction.

Fig.17 Profiles of ion current (●) and net current (▲) densities along the y axis observed at $z = 6$ cm in the case with a metal plate at $x = 2.5$ cm. The strength of $B_\perp$ is 2 kG.

Fig.18 Profile of ion current density along the y axis observed at $z = 6$ cm in the case with a metal plate at $x = 10$ cm. The strength of $B_\perp$ is 2 kG.

Fig.19 Electric field strength E as a function of position x of the metal plate obtained at $z = 0$ for $B_\perp = 1$ kG (closed plots) and $B_\perp = 2$ kG (open plots). Circles (triangles) are data points for $B_\perp$ in the + (-) x direction.

Fig.20 Arrangement of the probes and the metal plate for the experiment described in Section 4.C.(ii).

Fig.21 Axial distribution of electric field strength E near the entrance to the short-circuit region. Each closed (open) circle corresponds to the result

Fig.22 Relation between normalized electric field strength $E/\bar{u}_0 B_\perp$ and κ. Closed (open) circles are obtained from data at $B_\perp = 1$ kG ($B_\perp = 2$ kG).

of a single shot at $B_\perp = 1$ kG ($B_\perp = 2$ kG).

Fig.A1 Plots of u/u_0, $\delta y/\rho_i$ and $E_y/u_0 B_\perp$ as a function of distance $\nu z/u_0$ in the case of $\nu \ll 2\omega^*$. We have chosen $\nu/2\omega^* = 0.1$ and $\kappa = 100$ as an example.

Fig.A2 Plots of u/u_0, $\delta y/\rho_i$ and $E_y/u_0 B_\perp$ as a function of distance $\nu z/u_0$ in the case of $\nu = 2\omega^*$ ($\kappa = 100$).

Fig.A3 Plots of u/u_0, $\delta y/\rho_i$ and $E_y/u_0 B_\perp$ as a function of distance $\nu z/u_0$ in the case of $\nu \gg 2\omega^*$ ($\kappa = 100$).

Fig.B1 (a) Framing pictures of the light from the anode plasma taken from the side of the reflex triode.

(b) The field of view of framing camera.

(c) Correspondence of each framing picture to waveforms of anode voltage V and diode current I.

Fig.B2 (a) Framing pictures of the light from the anode plasma taken from the front of the reflex triode.

(b) The field of view of framing camera.

(c) Correspondence of each framing picture to waveforms of anode voltage V and diode current I.

Fig.B3 Framing pictures of the light from the anode plasma taken from the front of the reflex triode in the case without a cathode pin.

Fig.B4 Waveforms of anode voltage V and diode current I for the different strength of axial magnetic field B_z.

Fig.B5 Ion current detected at z = -13 cm as a function of the strength of axial magnetic field B_z.

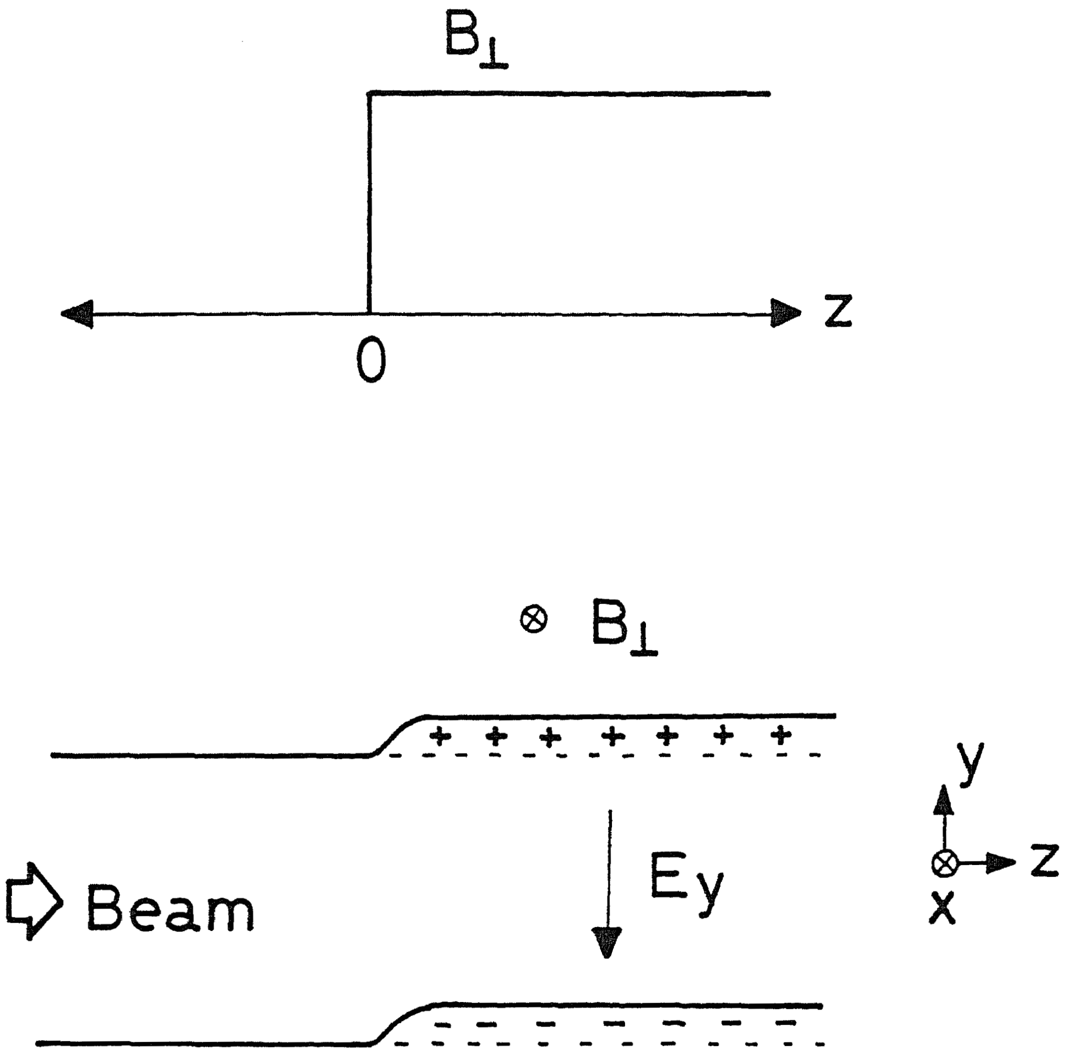

Fig. 1

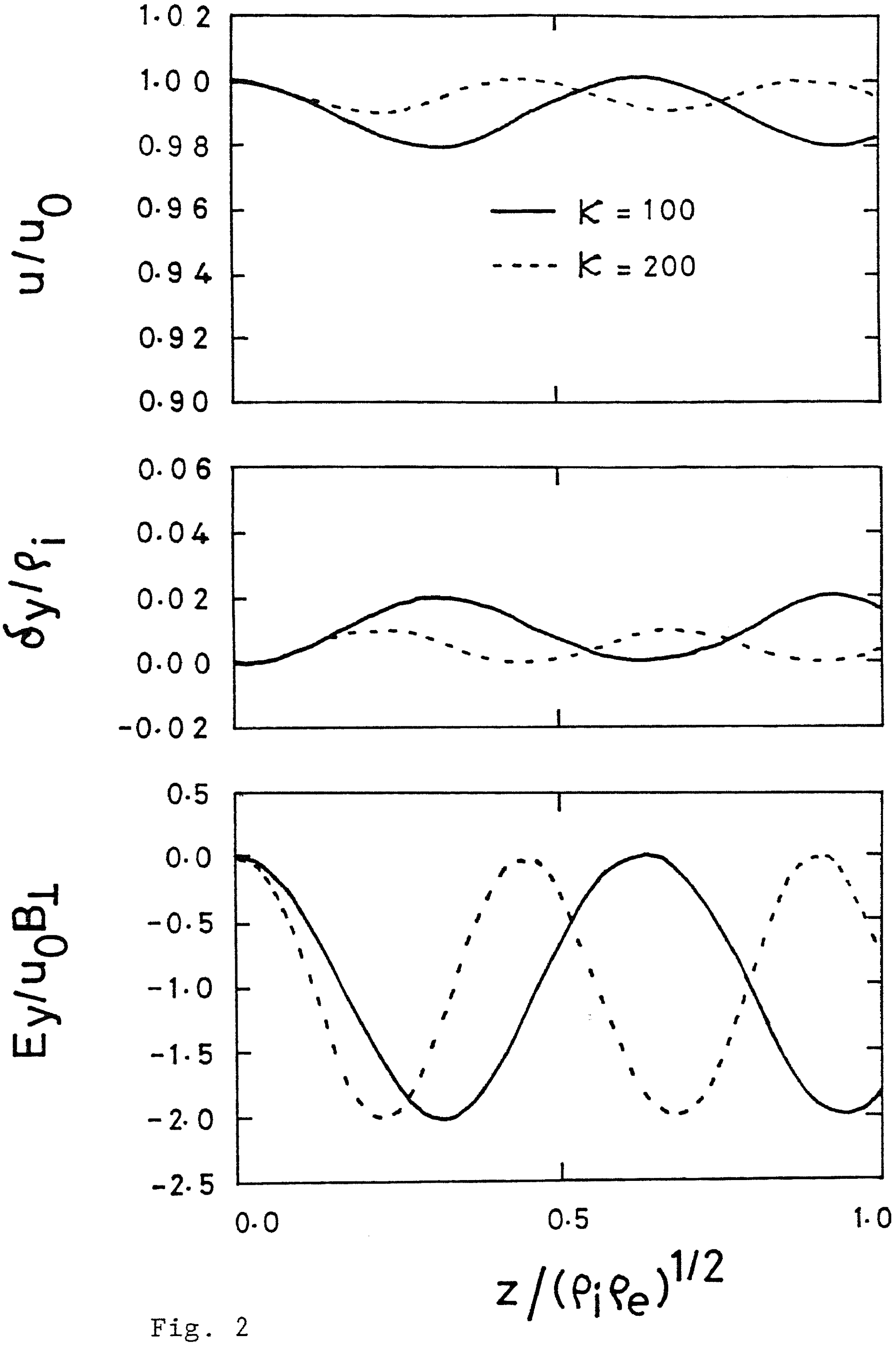

u/u$_0$
1·02
1·00
0·98
0·96
0·94
0·92
0·90
K = 100
K = 200
δy/ρ$_i$
0·06
0·04
0·02
0·00
-0·02
Ey/u$_0$B$_⊥$
0·5
0·0
-0·5
-1·0
-1·5
-2·0
-2·5
0·0
0·5
1·0
z/(ρ$_i$ρ$_e$)$^{1/2}$

Fig. 2

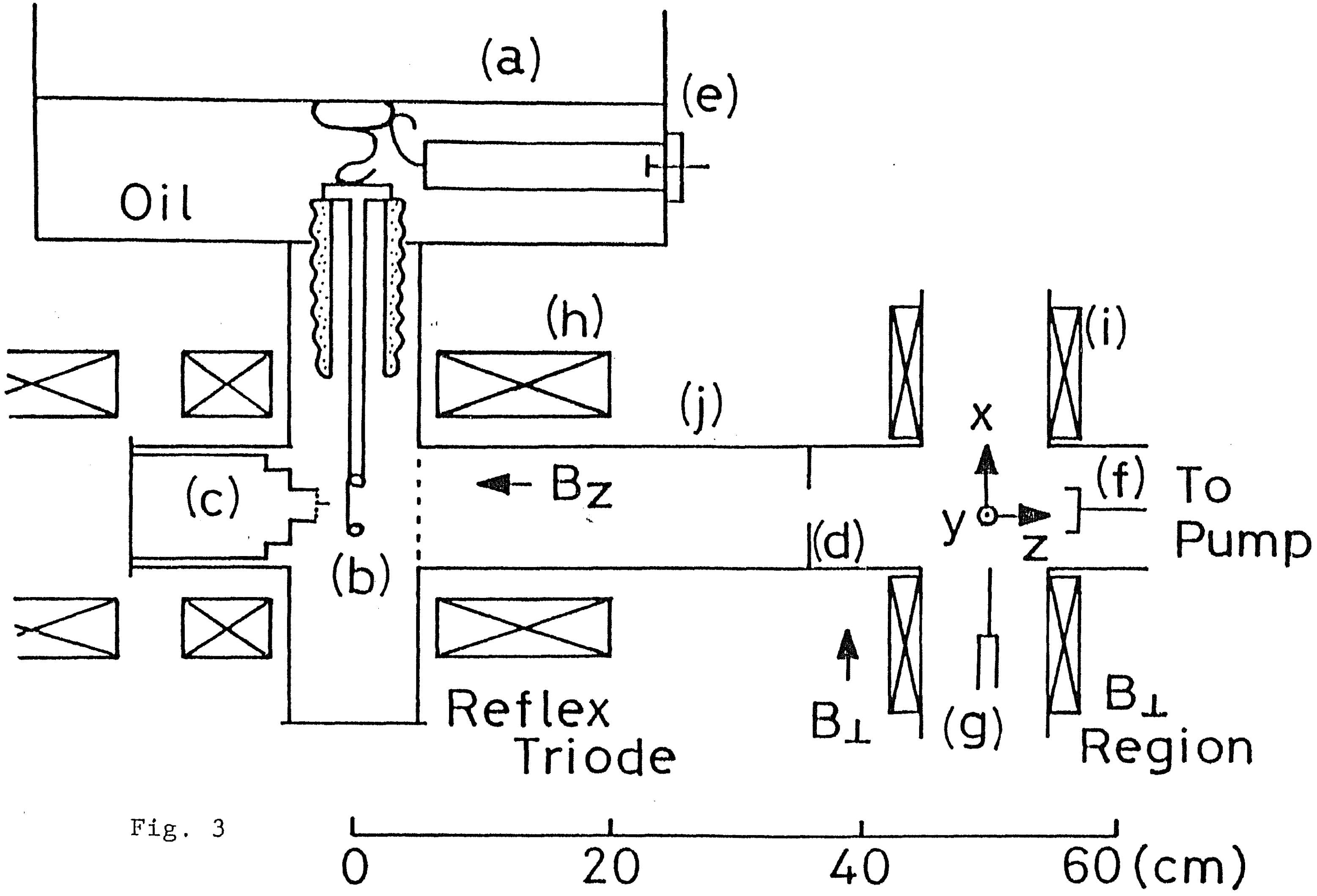
(a)
(e)
Oil
(h)
(i)
(j)
x
(f)
To
Pump
(c)
$\leftarrow B_Z$
y
z
(d)
(b)
$B_\perp$
(g)
$B_\perp$
Region
Reflex
Triode
0
20
40
60 (cm)

Fig. 3

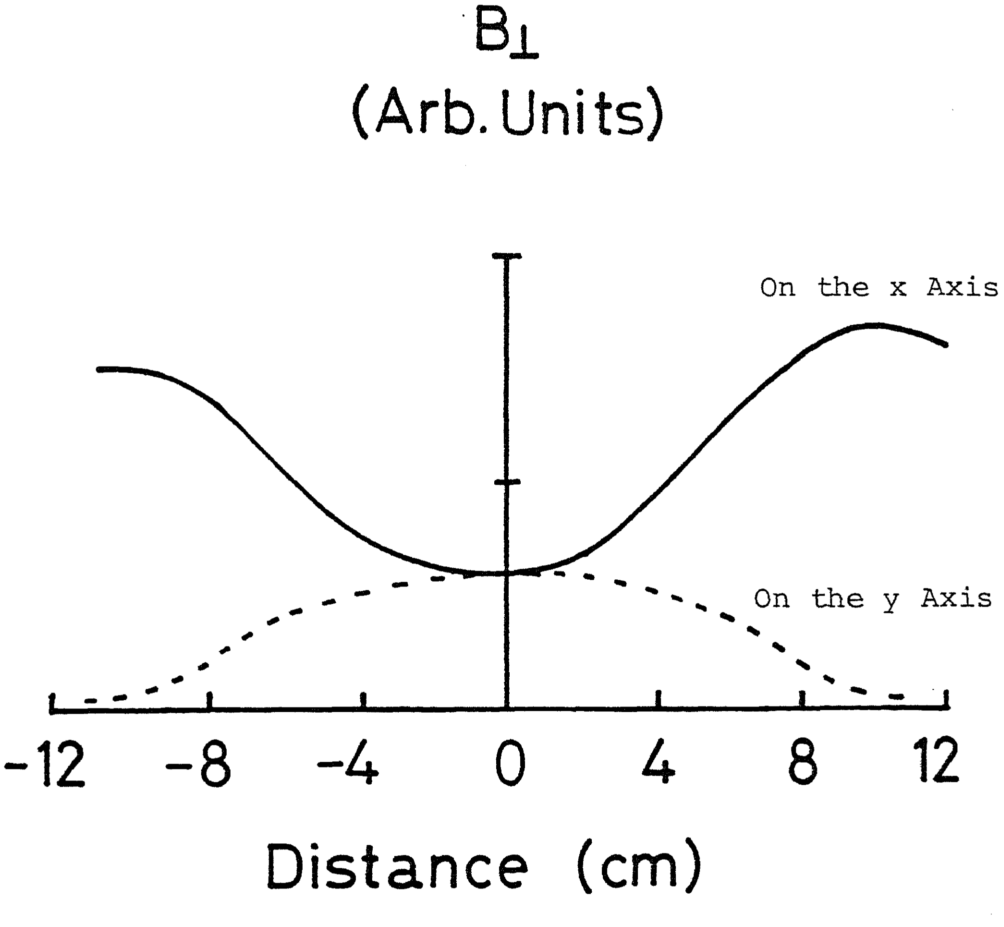
$B_{\perp}$
(Arb. Units)
On the x Axis
On the y Axis
-12
-8
-4
0
4
8
12
Distance (cm)

Fig. 4

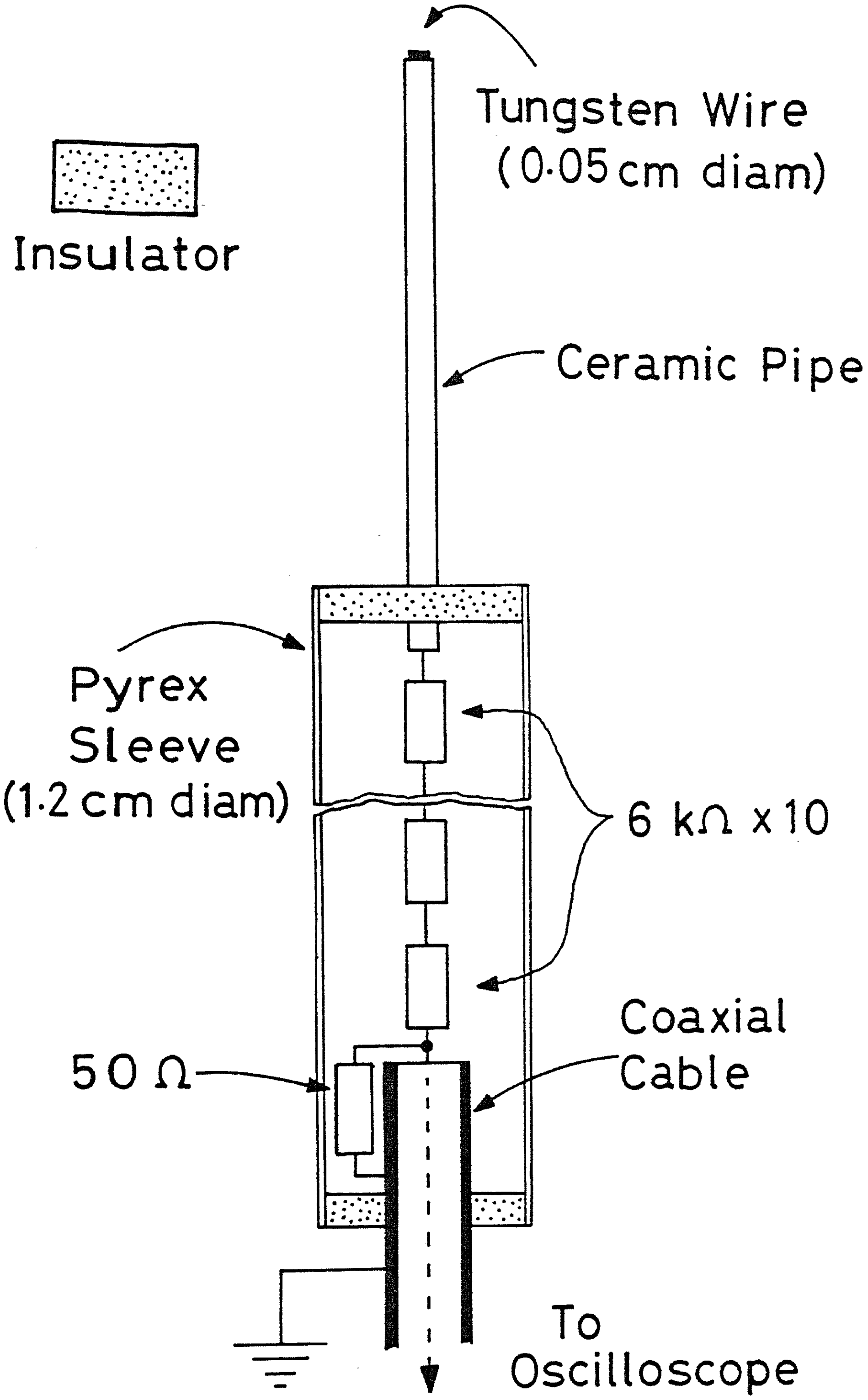
Tungsten Wire
(0·05 cm diam)
Insulator
Ceramic Pipe
Pyrex
Sleeve
(1·2 cm diam)
6 kΩ x10
Coaxial
Cable
50 Ω
To
Oscilloscope

Fig. 5

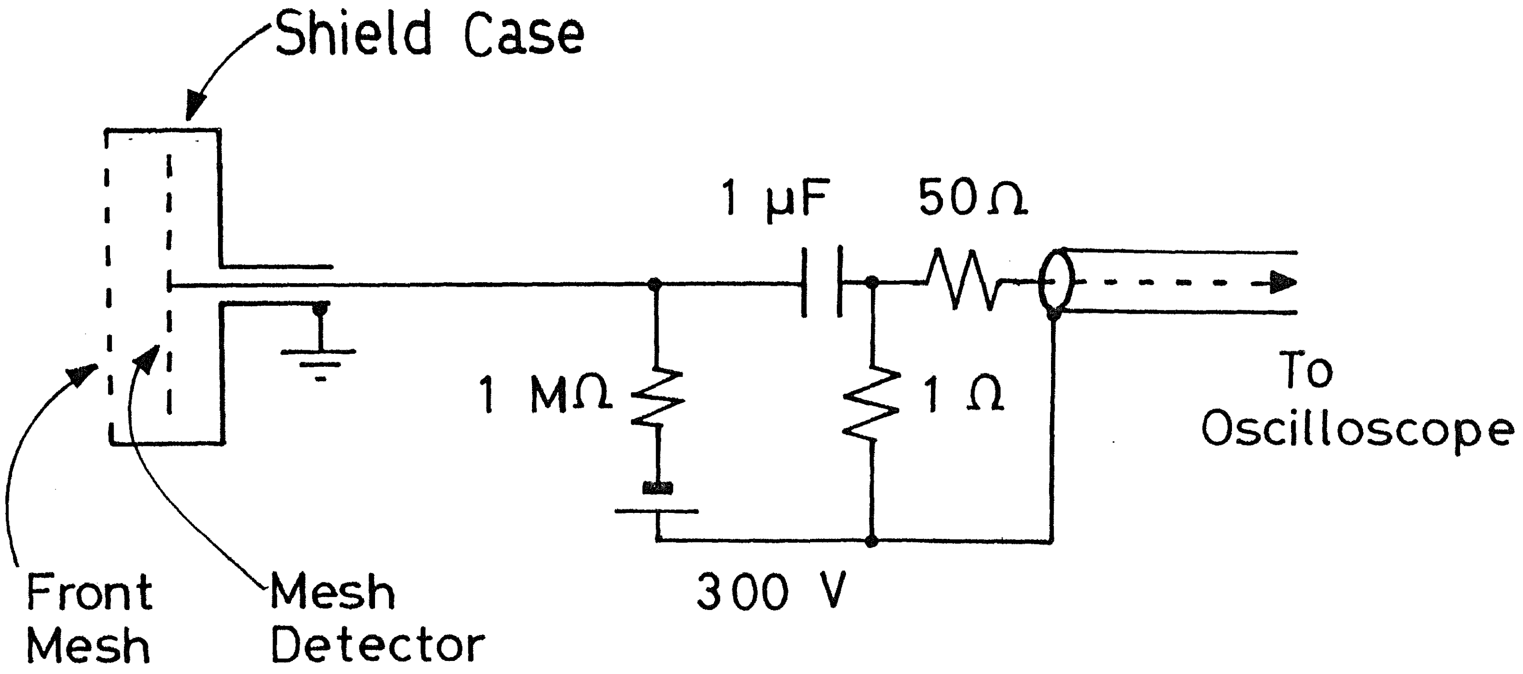
Shield Case
1 μF
50Ω
1 MΩ
1 Ω
To
Oscilloscope
Front
Mesh
Mesh
Detector
300 V

Fig. 6

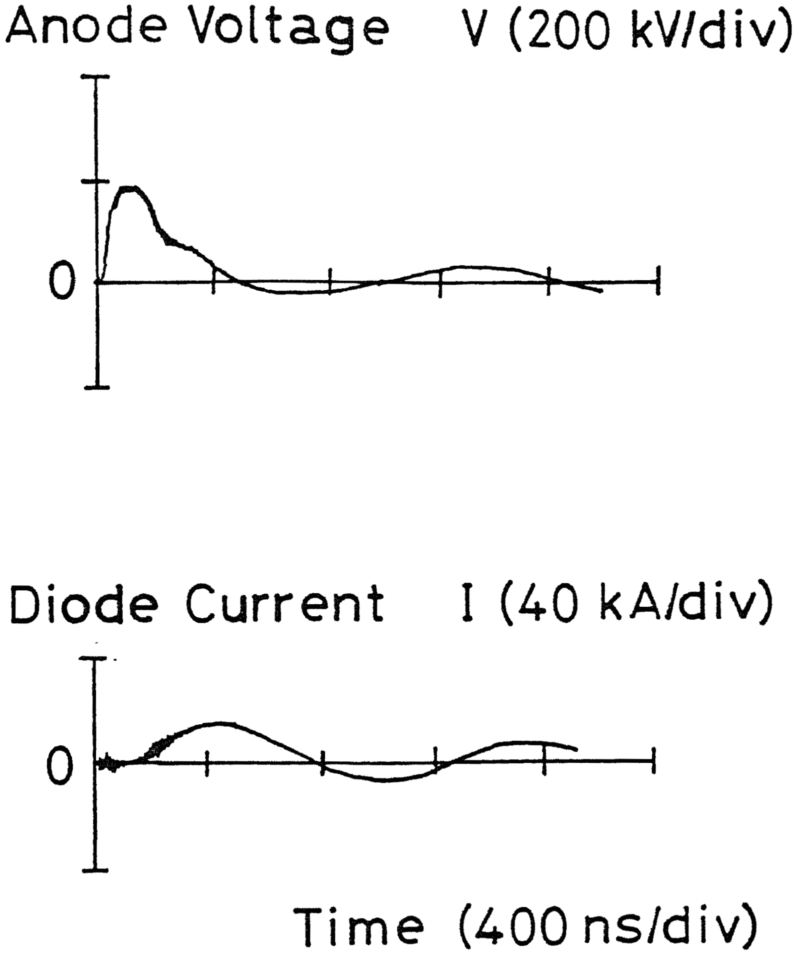
Anode Voltage V (200 kV/div)
0
Diode Current I (40 kA/div)
0
Time (400 ns/div)

Fig. 7

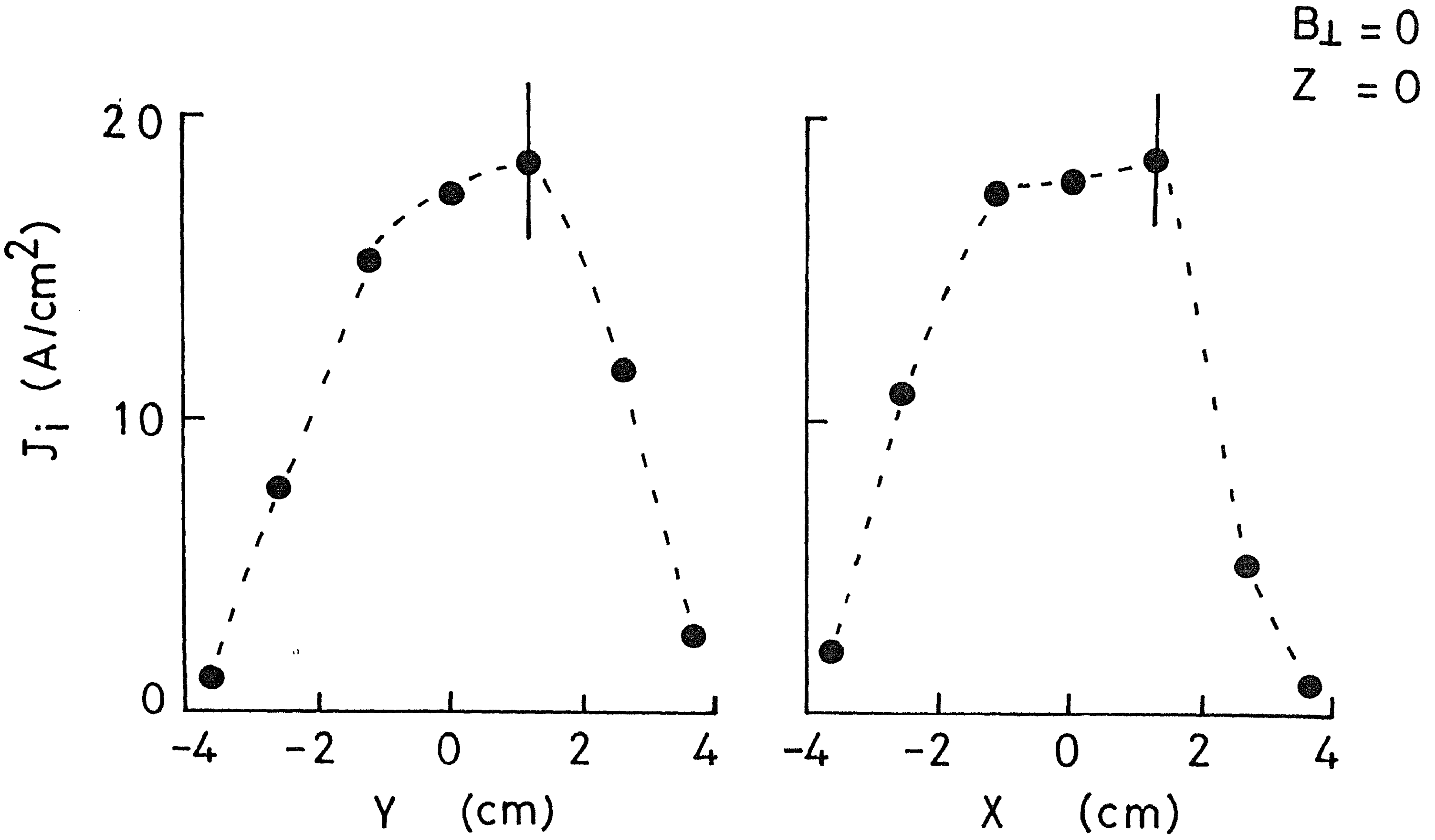

Fig. 8

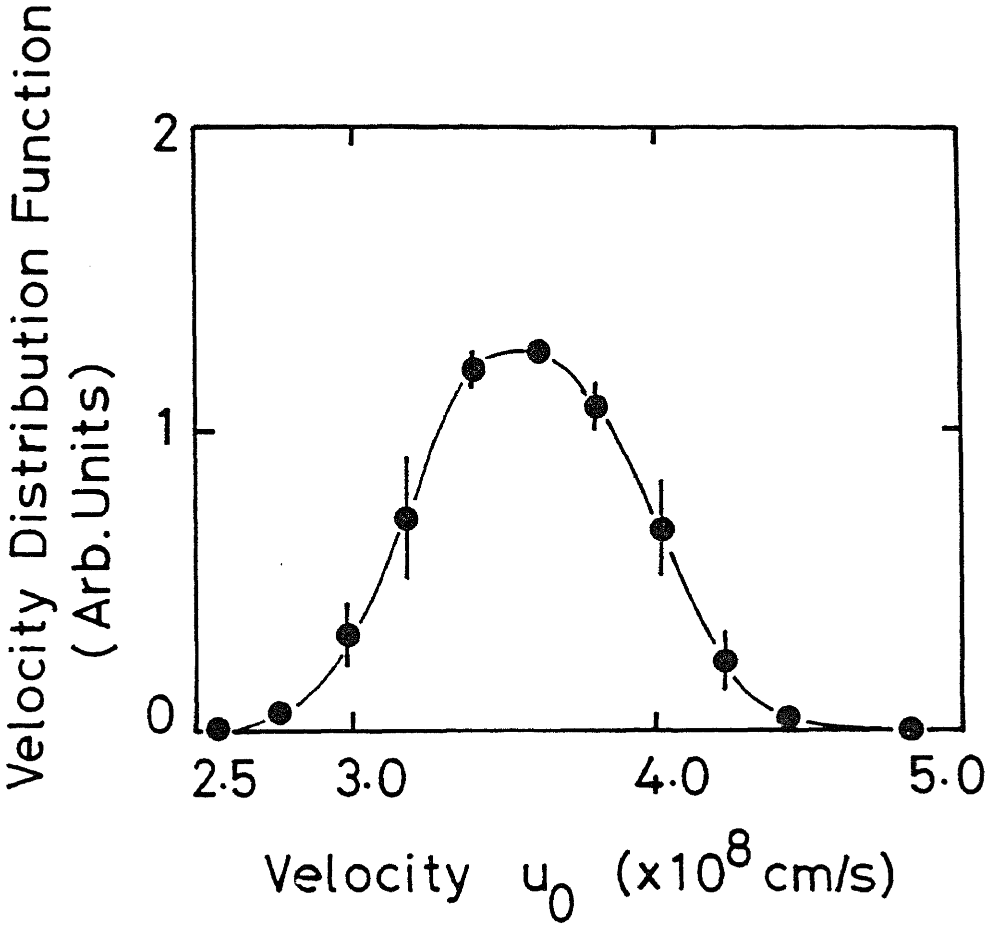
Velocity Distribution Function
(Arb.Units)
2
1
0
2.5
3.0
4.0
5.0
Velocity u_0 ($\times 10^8$ cm/s)

Fig. 9

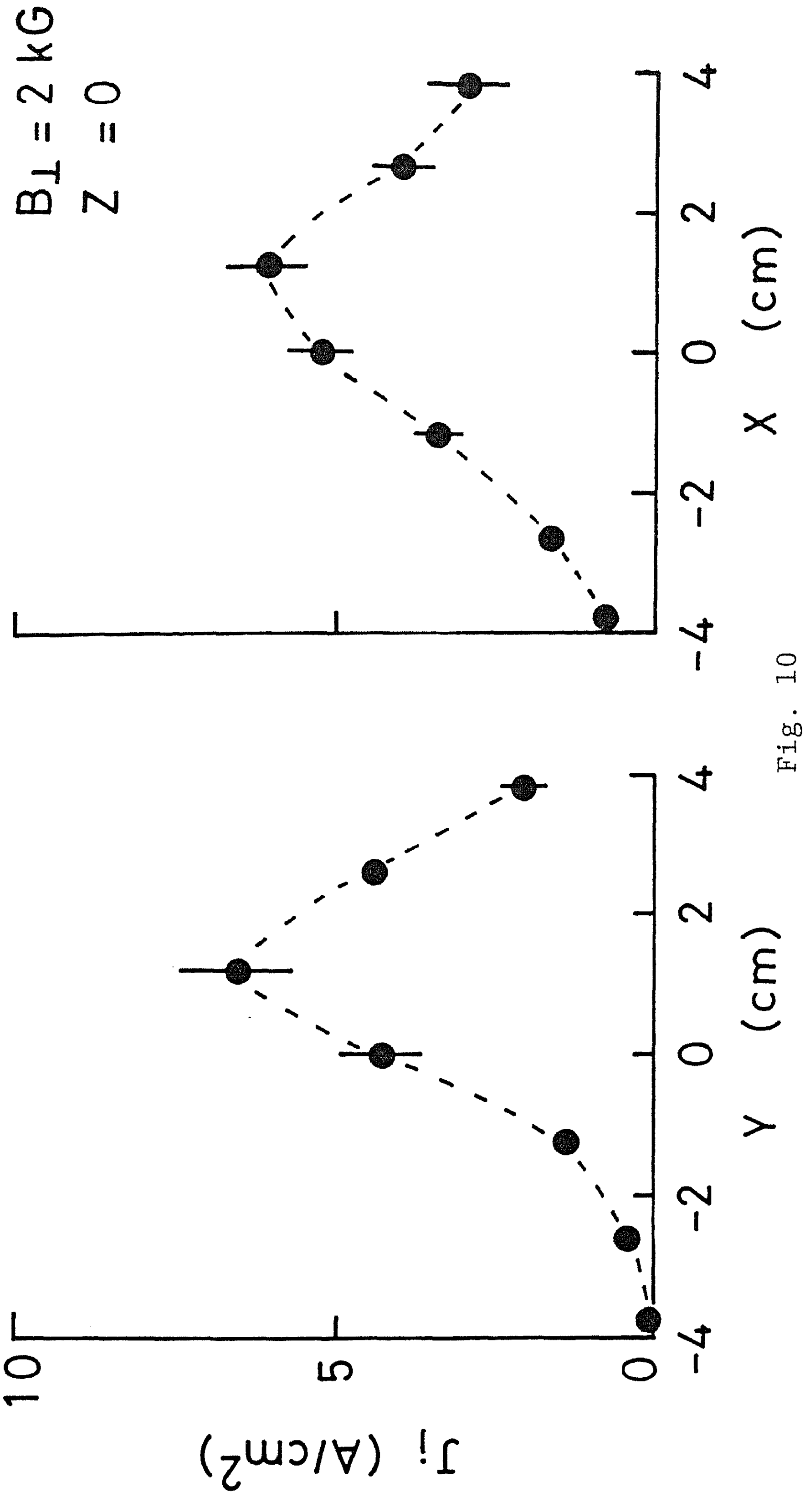

Fig. 10

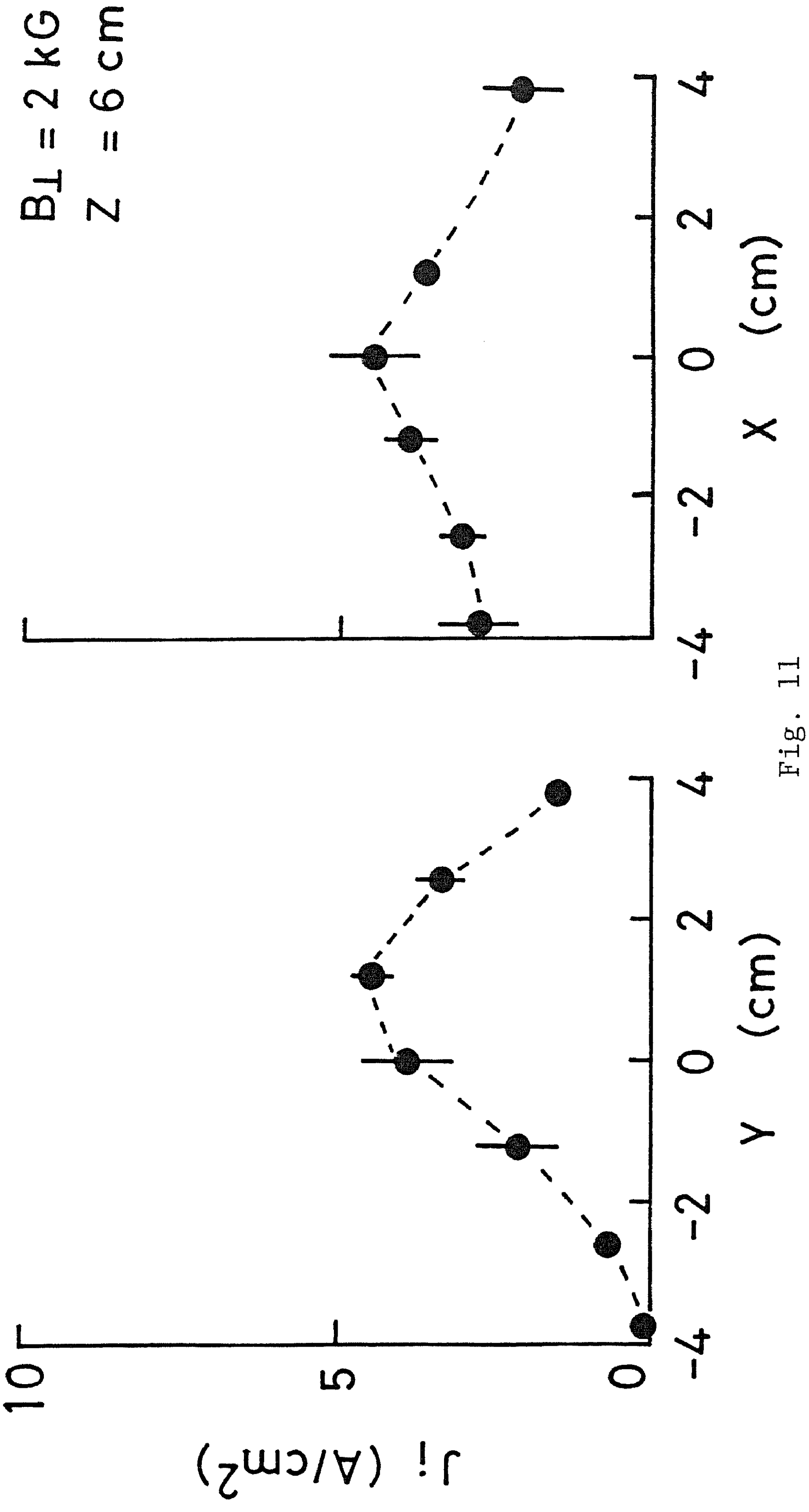

Fig. 11

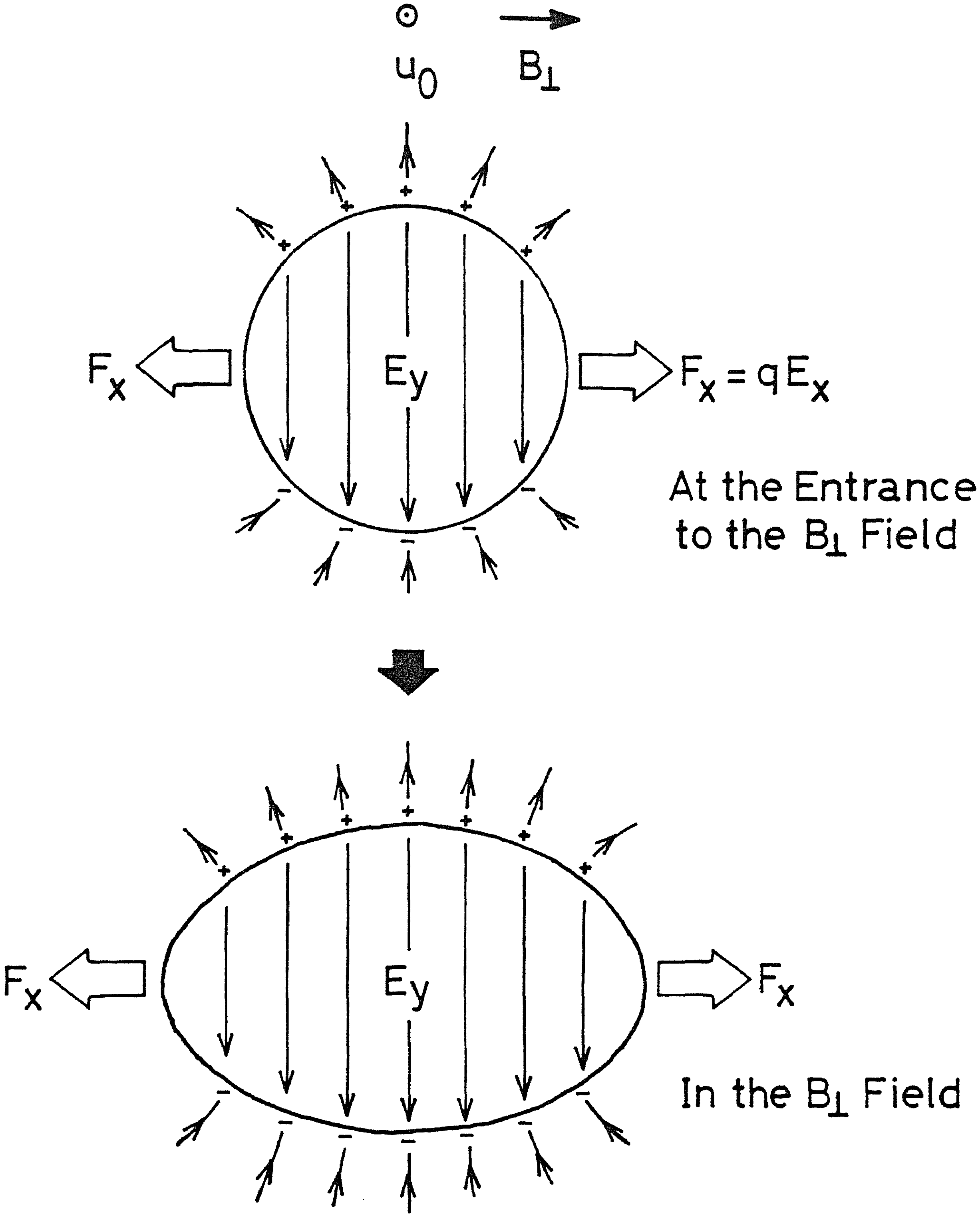
u₀
B⊥
Fx
Ey
Fx = qEx
At the Entrance to the B⊥ Field
Fx
Ey
Fx
In the B⊥ Field

Fig. 12

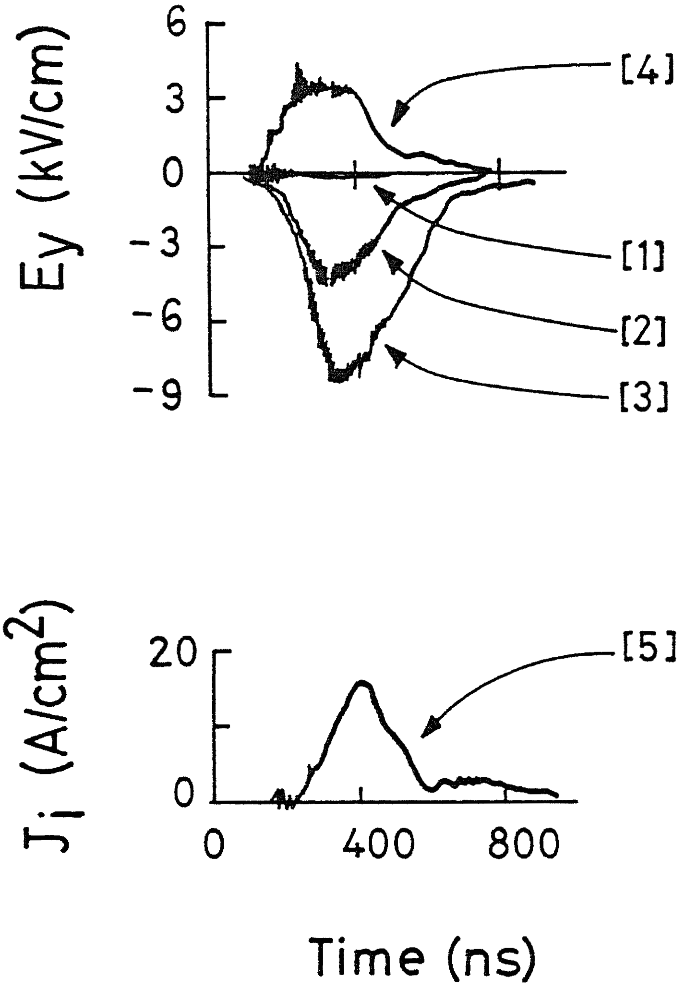

Fig. 13

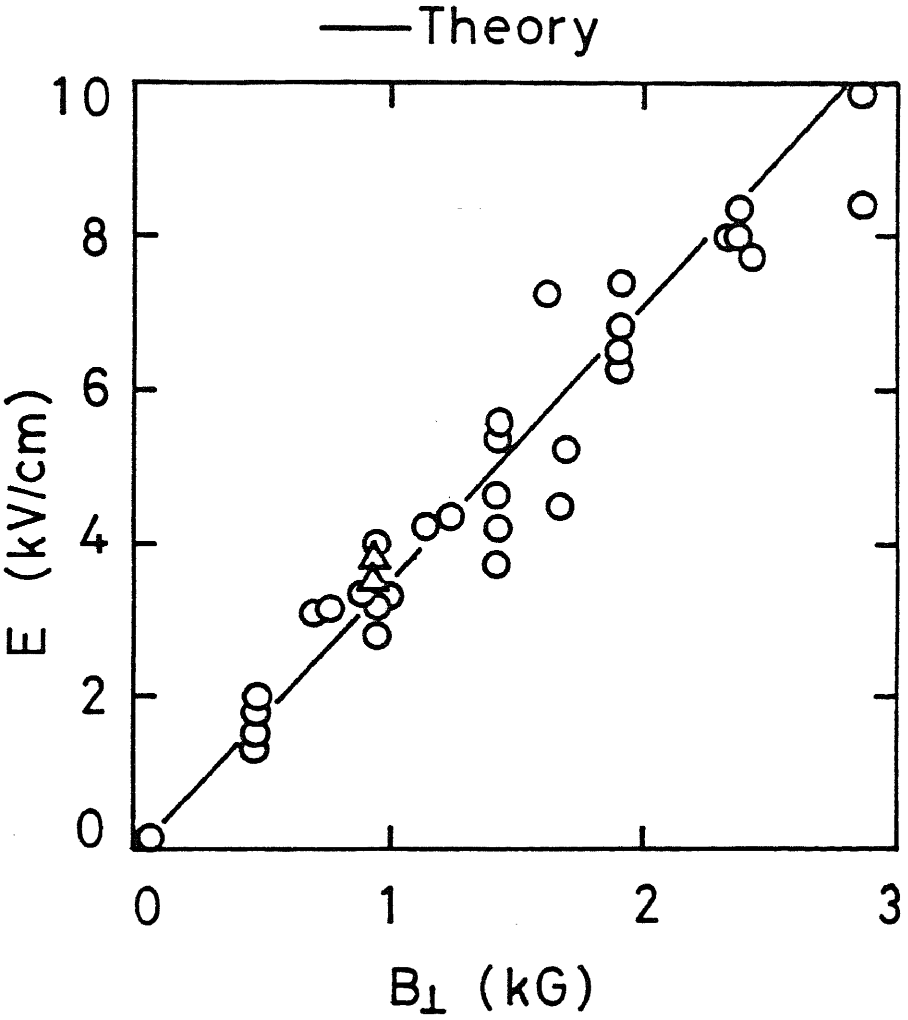

Fig. 14

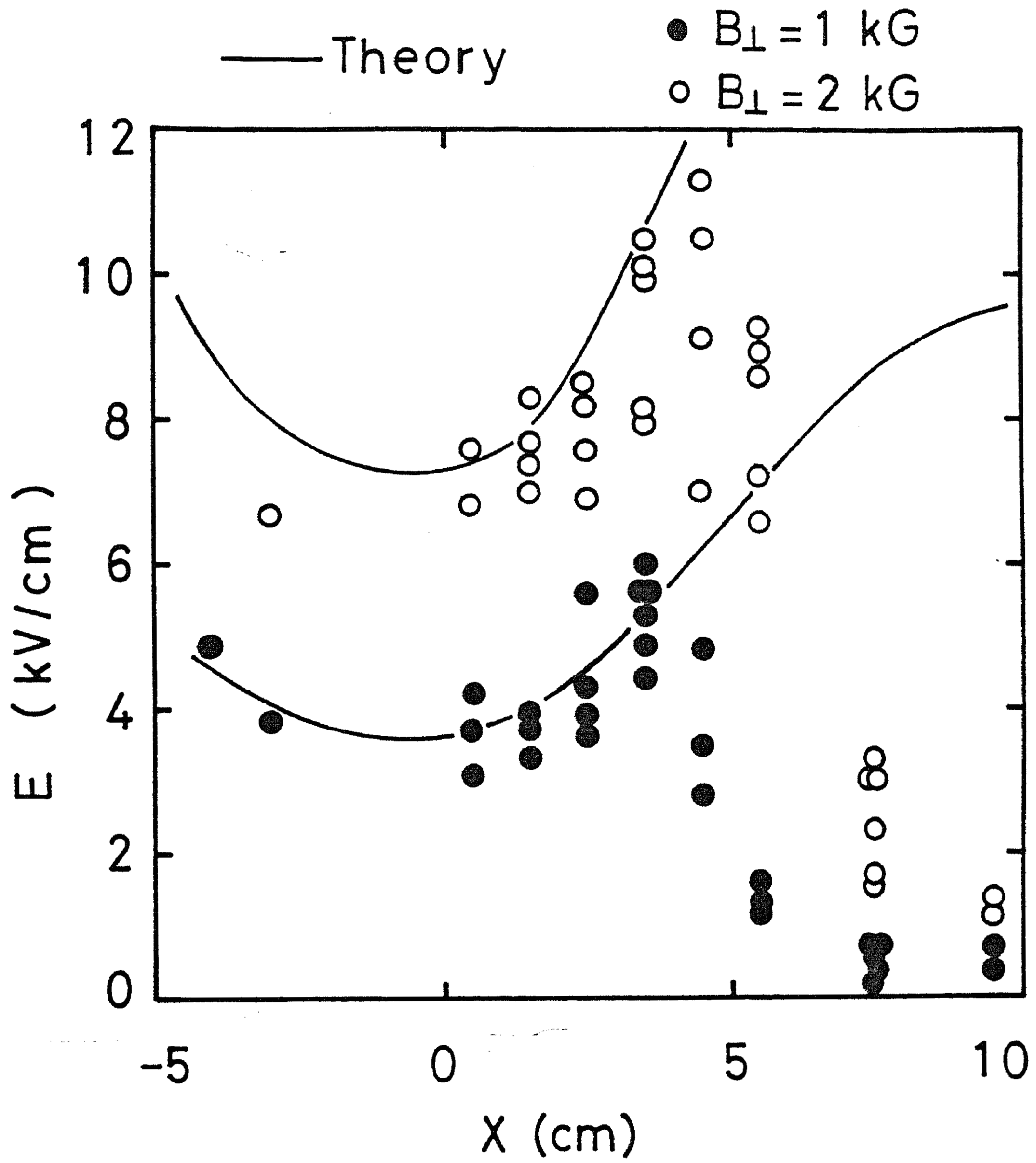

Fig. 15

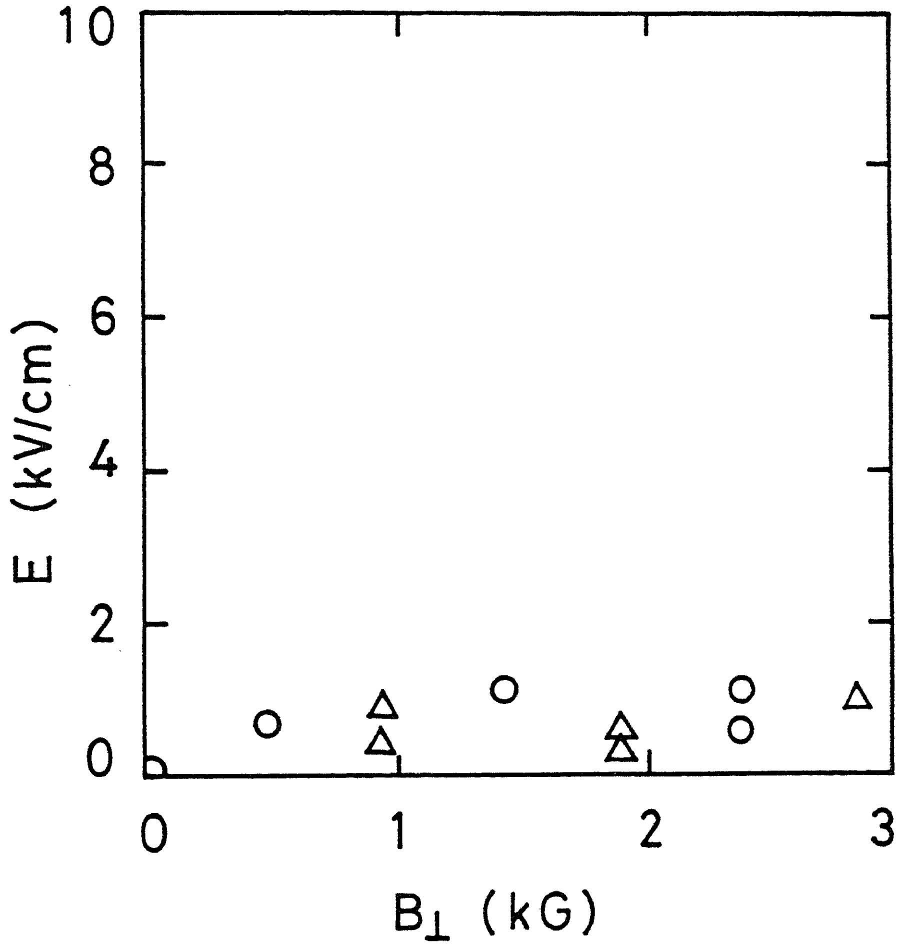

Fig. 16

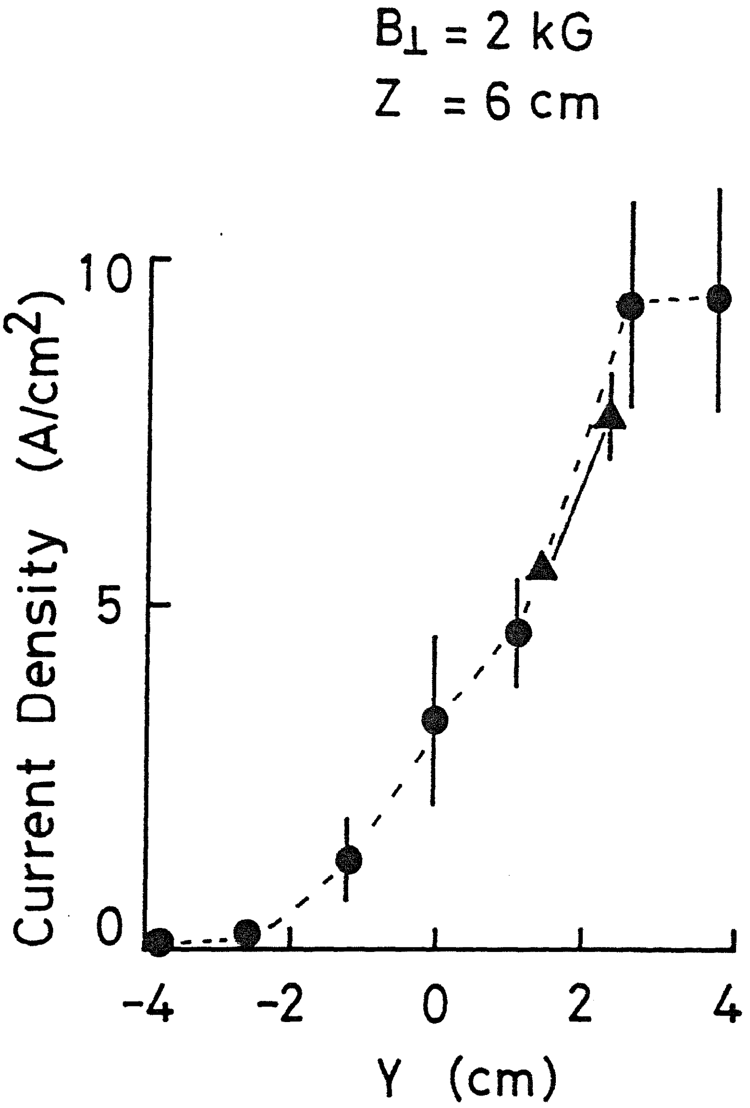

Fig. 17

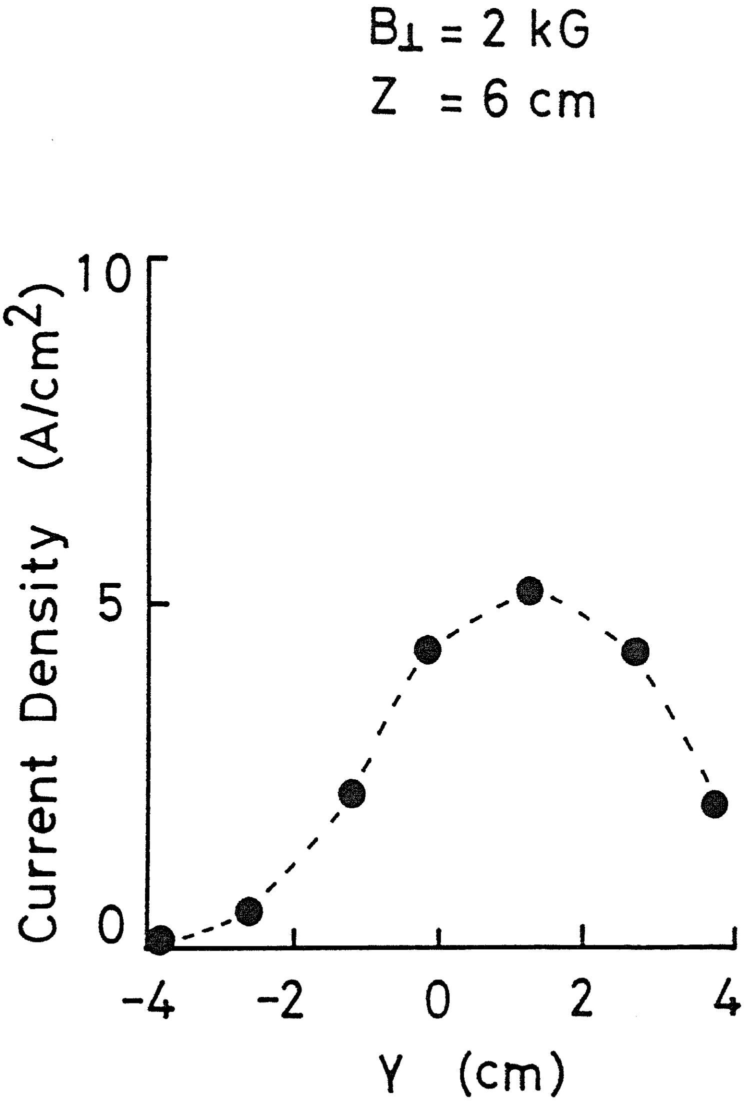

Fig. 18

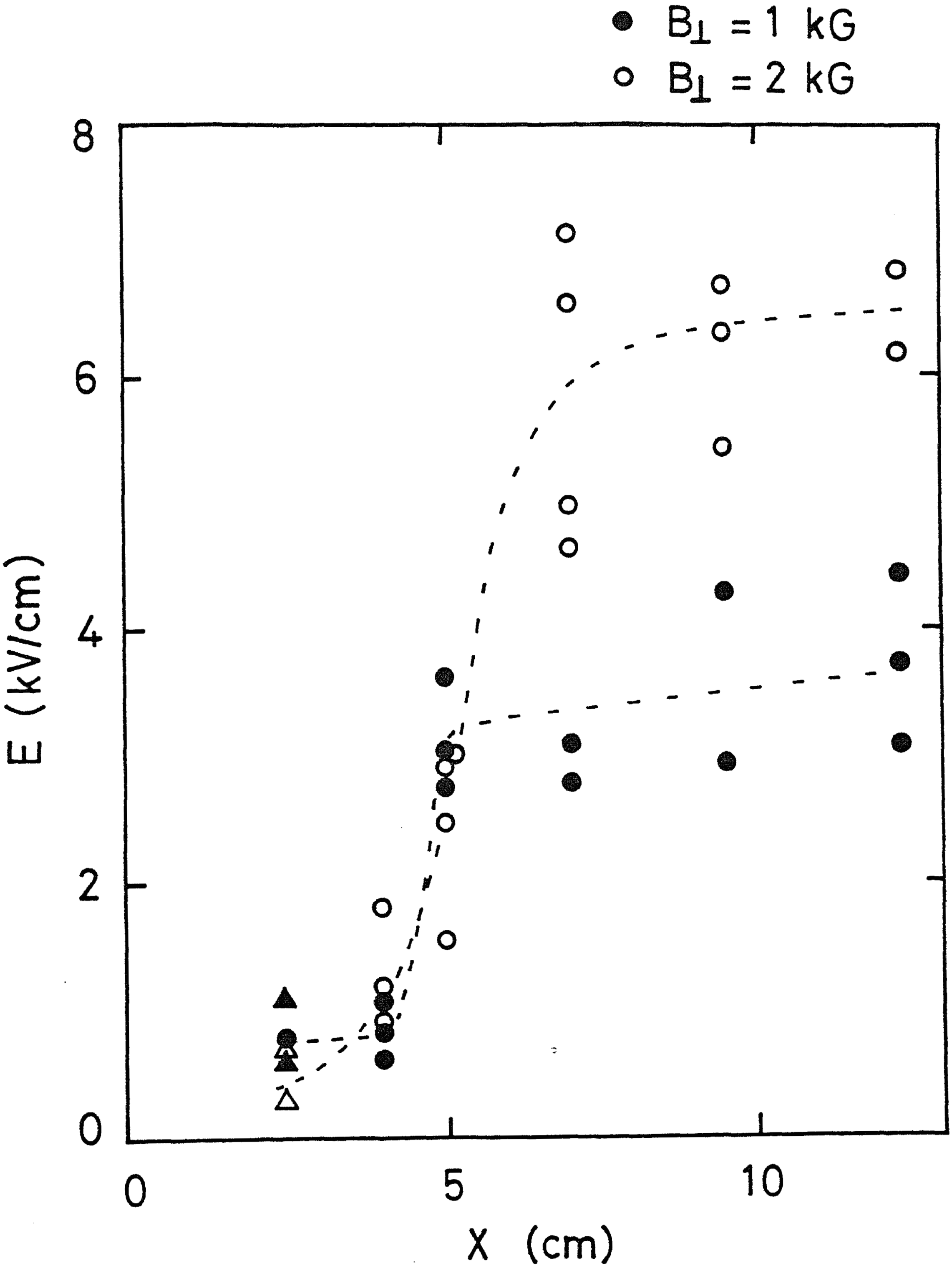

Fig. 19

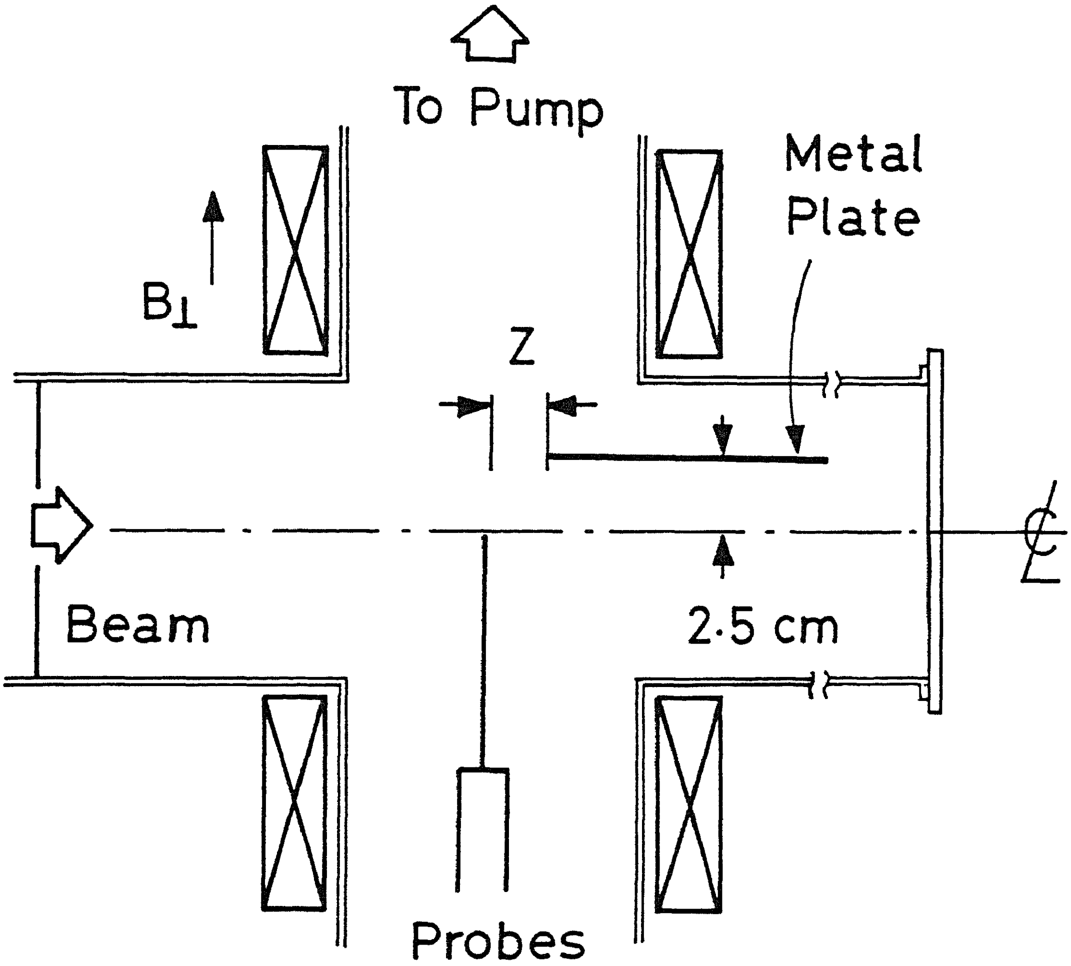

Fig. 20

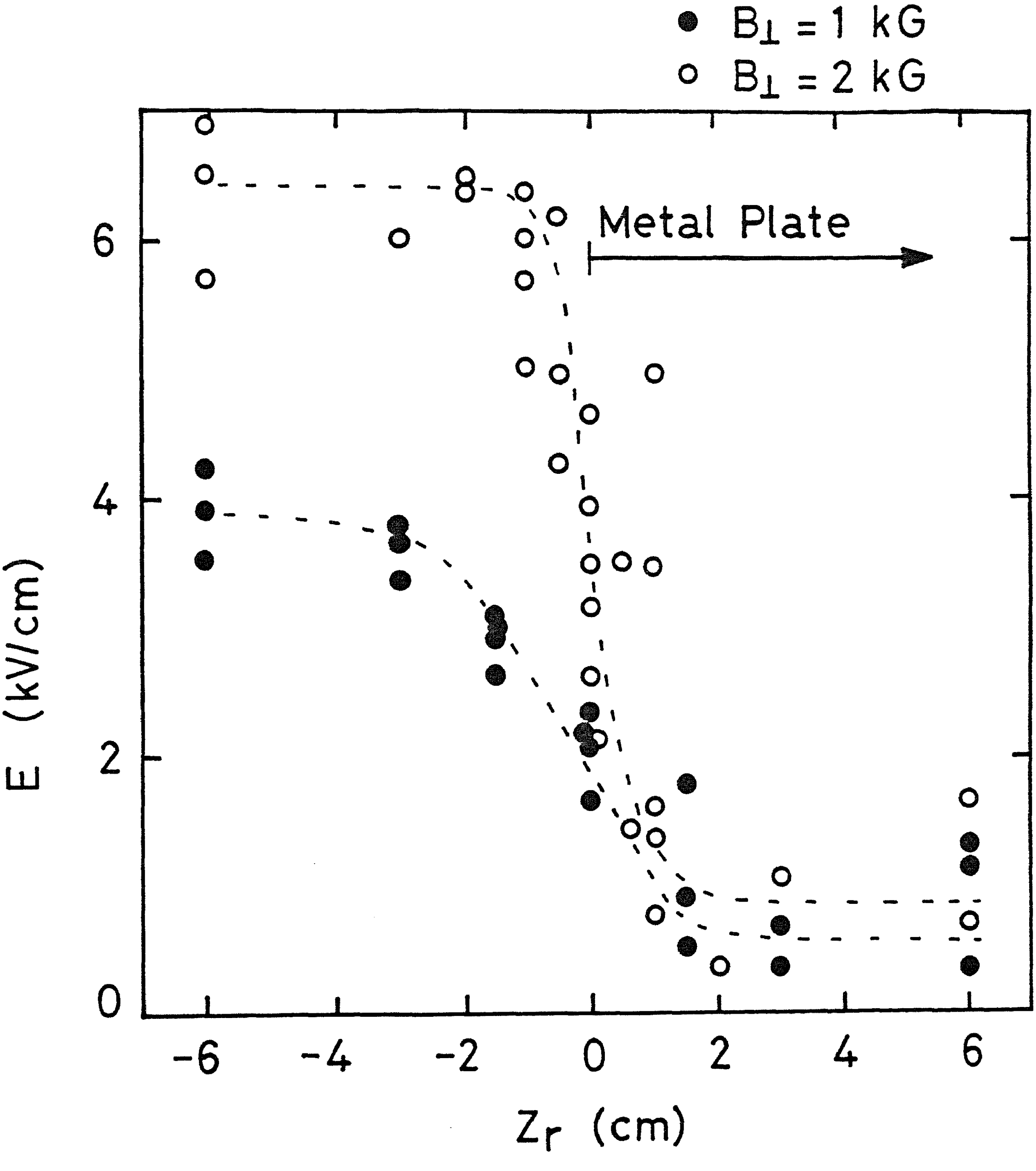

Fig. 21

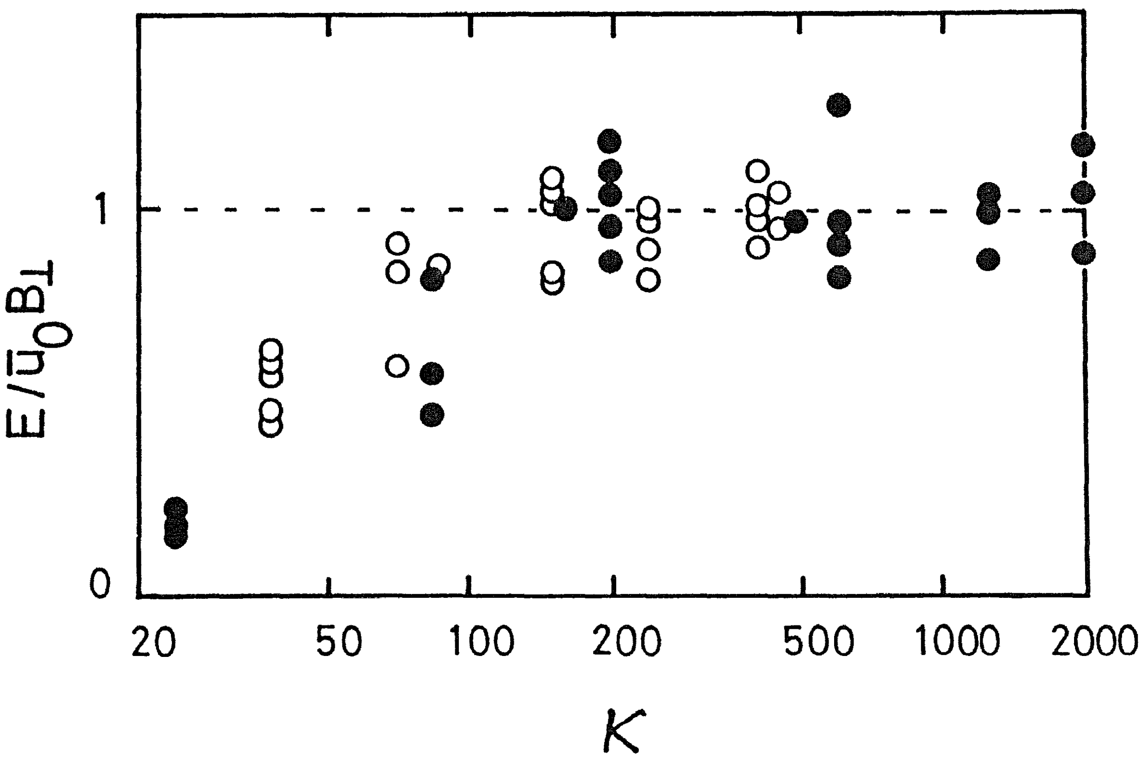

Fig. 22

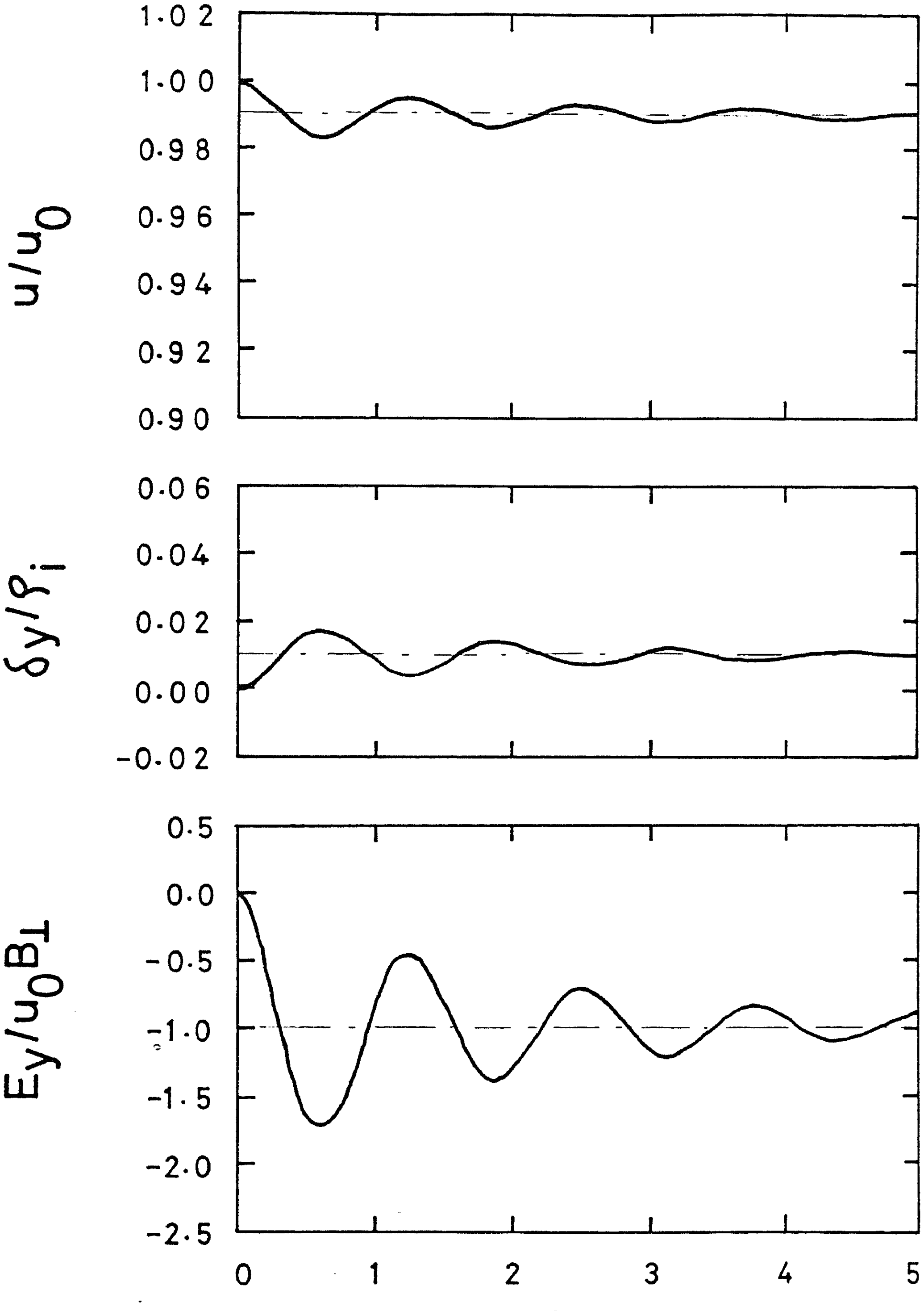

1·02
1·00
0·98
0·96
0·94
0·92
0·90
u/u_0
0·06
0·04
0·02
0·00
-0·02
$\delta y/\rho_i$
0·5
0·0
-0·5
-1·0
-1·5
-2·0
-2·5
$E_y/u_0B_\perp$
0
1
2
3
4
5
$\nu z/u_0$

Fig. A1

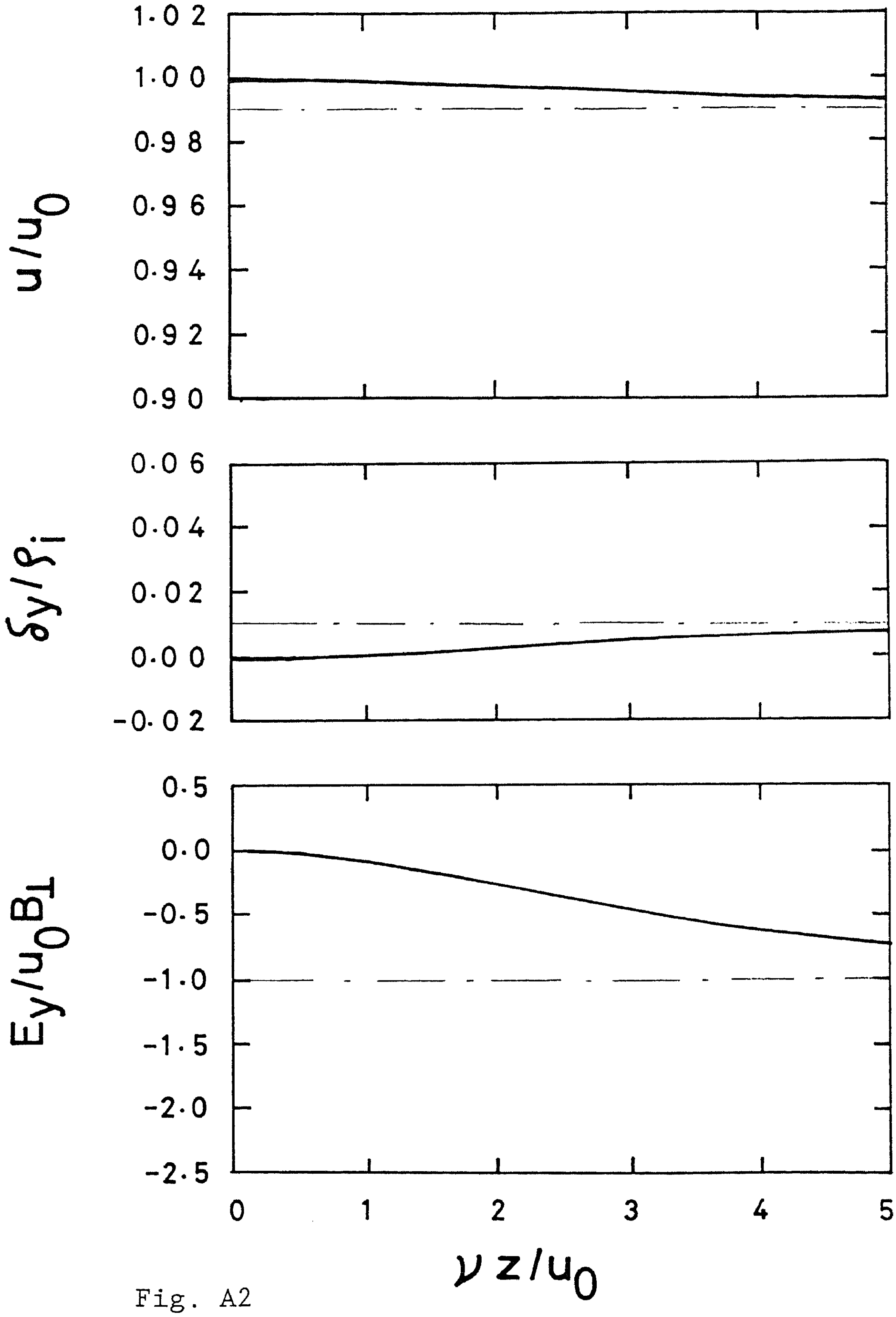
1·02
1·00
0·98
0·96
0·94
0·92
0·90
u/u_0
0·06
0·04
0·02
0·00
-0·02
$\delta y/\rho_i$
0·5
0·0
-0·5
-1·0
-1·5
-2·0
-2·5
$E_y/u_0B_\perp$
0
1
2
3
4
5
$\nu z/u_0$

Fig. A2

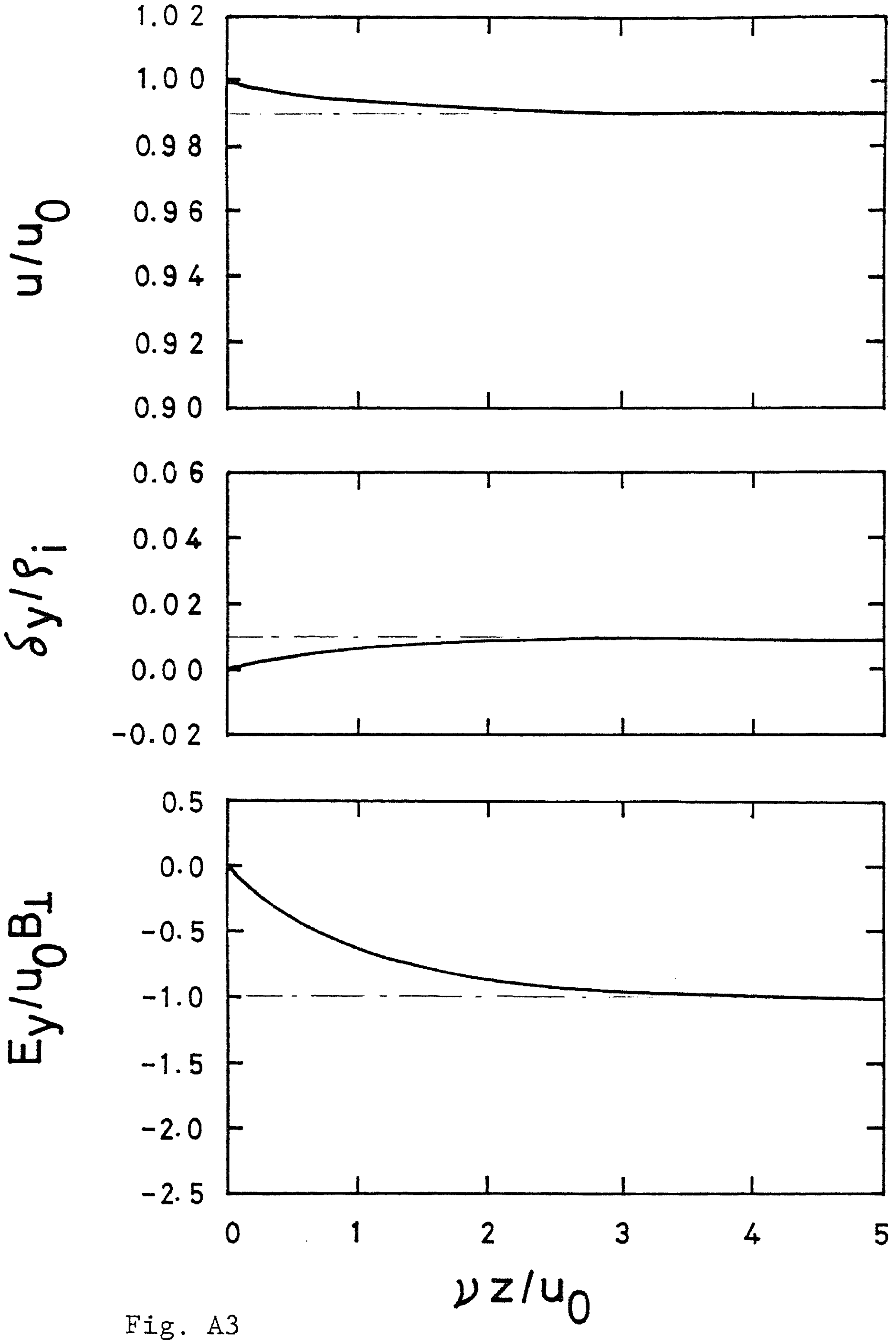
1.0 2
1.0 0
0.9 8
0.9 6
0.9 4
0.9 2
0.9 0
u/u_0
0.0 6
0.0 4
0.0 2
0.0 0
-0.0 2
δy/ρ_i
0.5
0.0
-0.5
-1.0
-1.5
-2.0
-2.5
E_y/u_0B_⊥
0
1
2
3
4
5
νz/u_0

Fig. A3

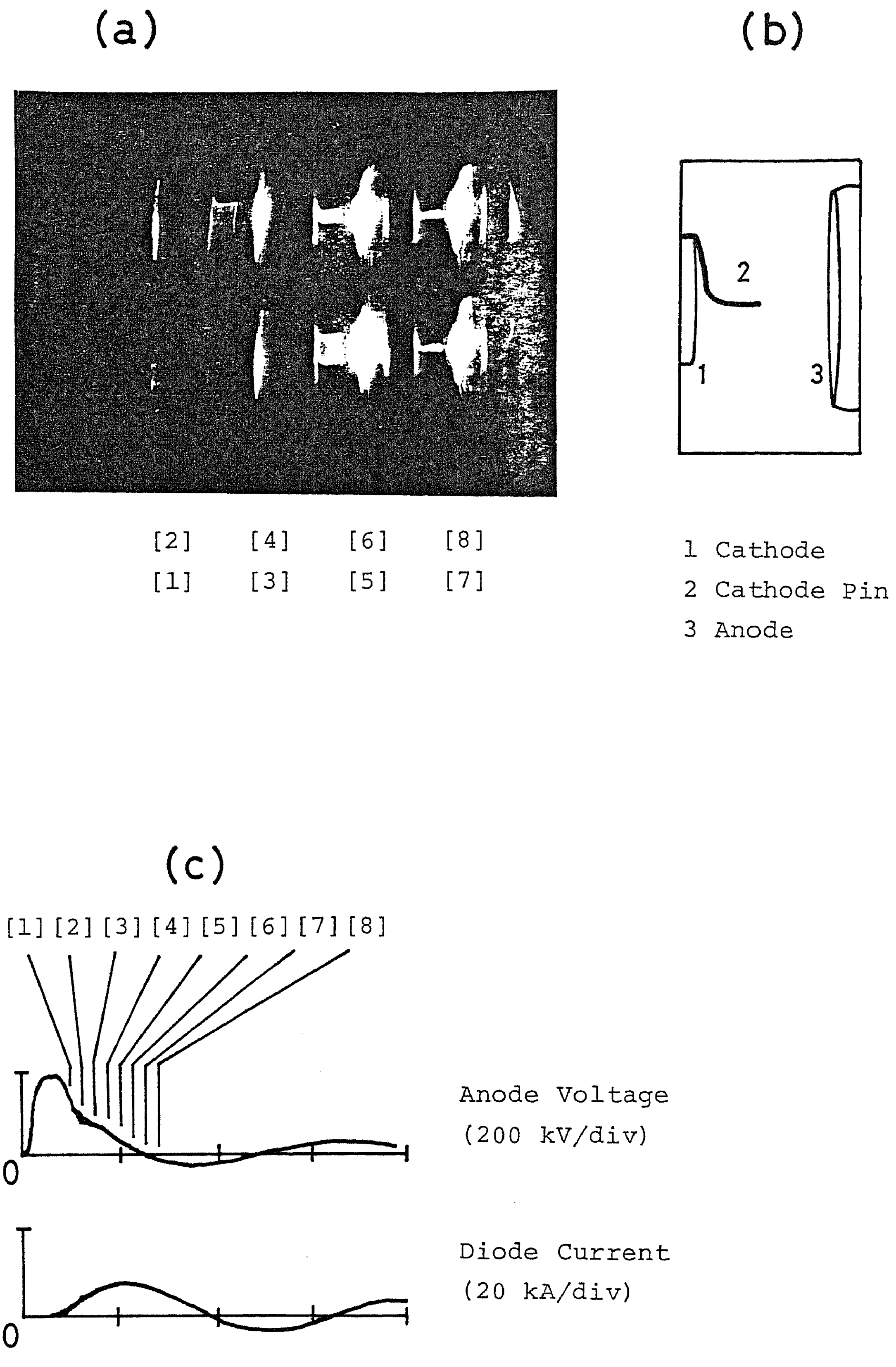
(a)
(b)
[2] [4] [6] [8]
[1] [3] [5] [7]
2
1
3
1 Cathode
2 Cathode Pin
3 Anode
(c)
[1] [2] [3] [4] [5] [6] [7] [8]
0
Anode Voltage
(200 kV/div)
0
Diode Current
(20 kA/div)
Time (400 ns/div)

Fig. B1

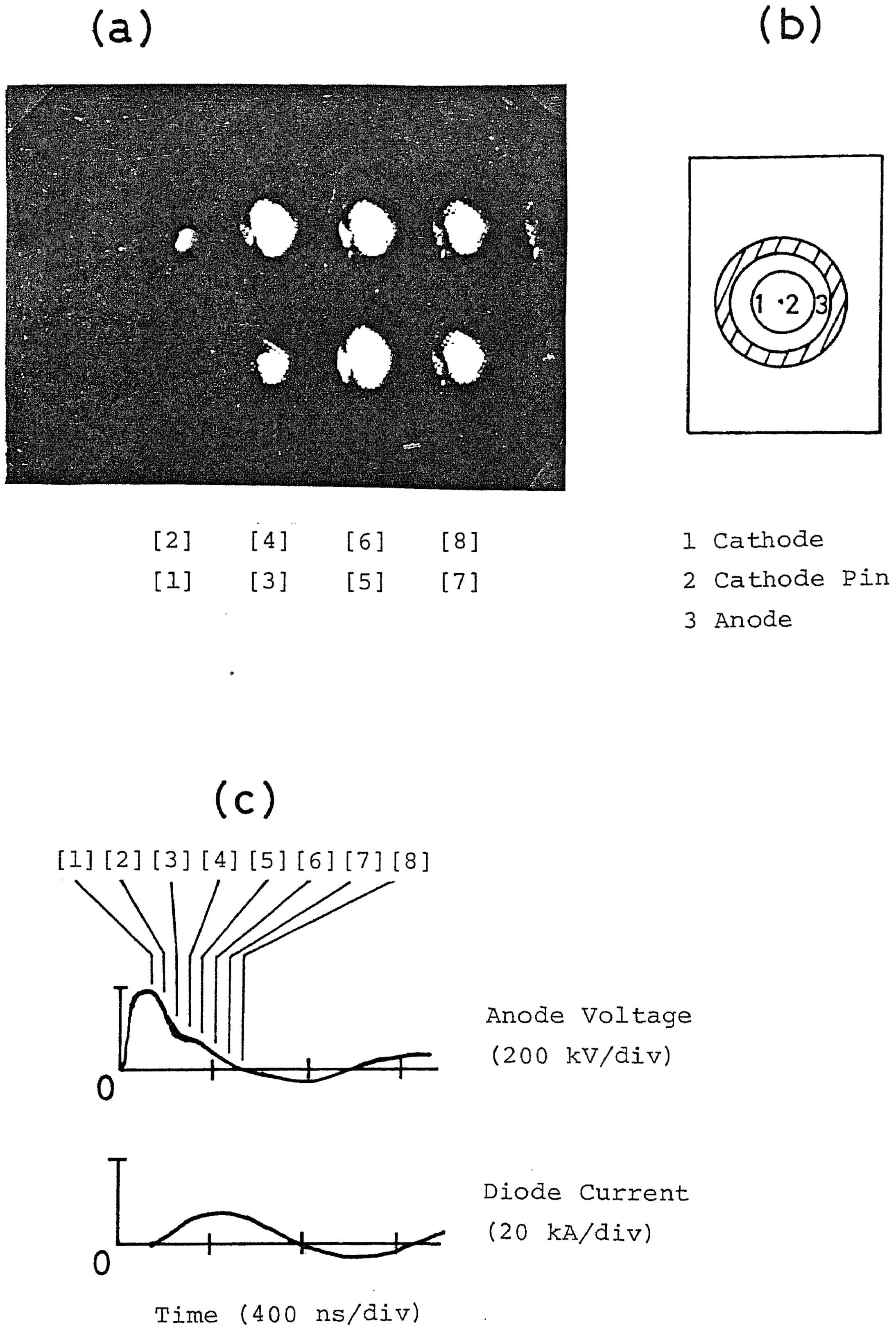
(a)
(b)
[2] [4] [6] [8]
[1] [3] [5] [7]
1
2
3
1 Cathode
2 Cathode Pin
3 Anode
(c)
[1] [2] [3] [4] [5] [6] [7] [8]
0
Anode Voltage
(200 kV/div)
0
Diode Current
(20 kA/div)
Time (400 ns/div)

Fig. B2

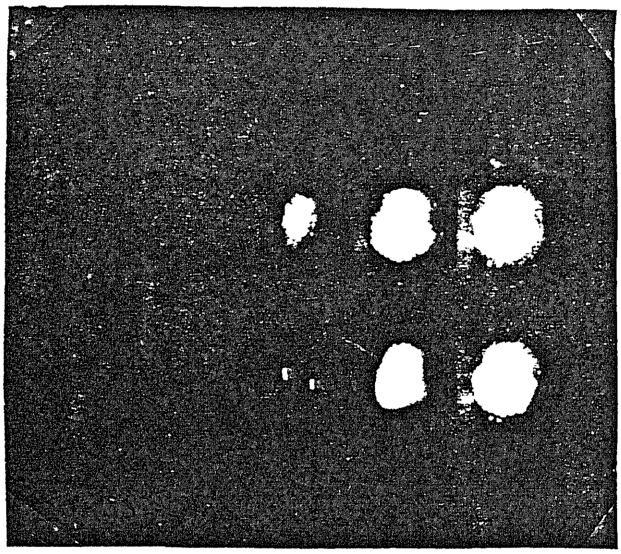

The Field of View of Framing Camera

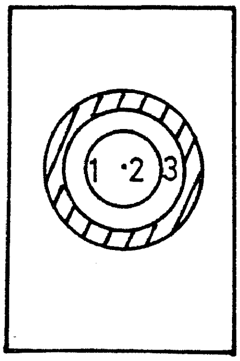

1 Cathode
2 Cathode Pin
3 Anode

Fig. B3

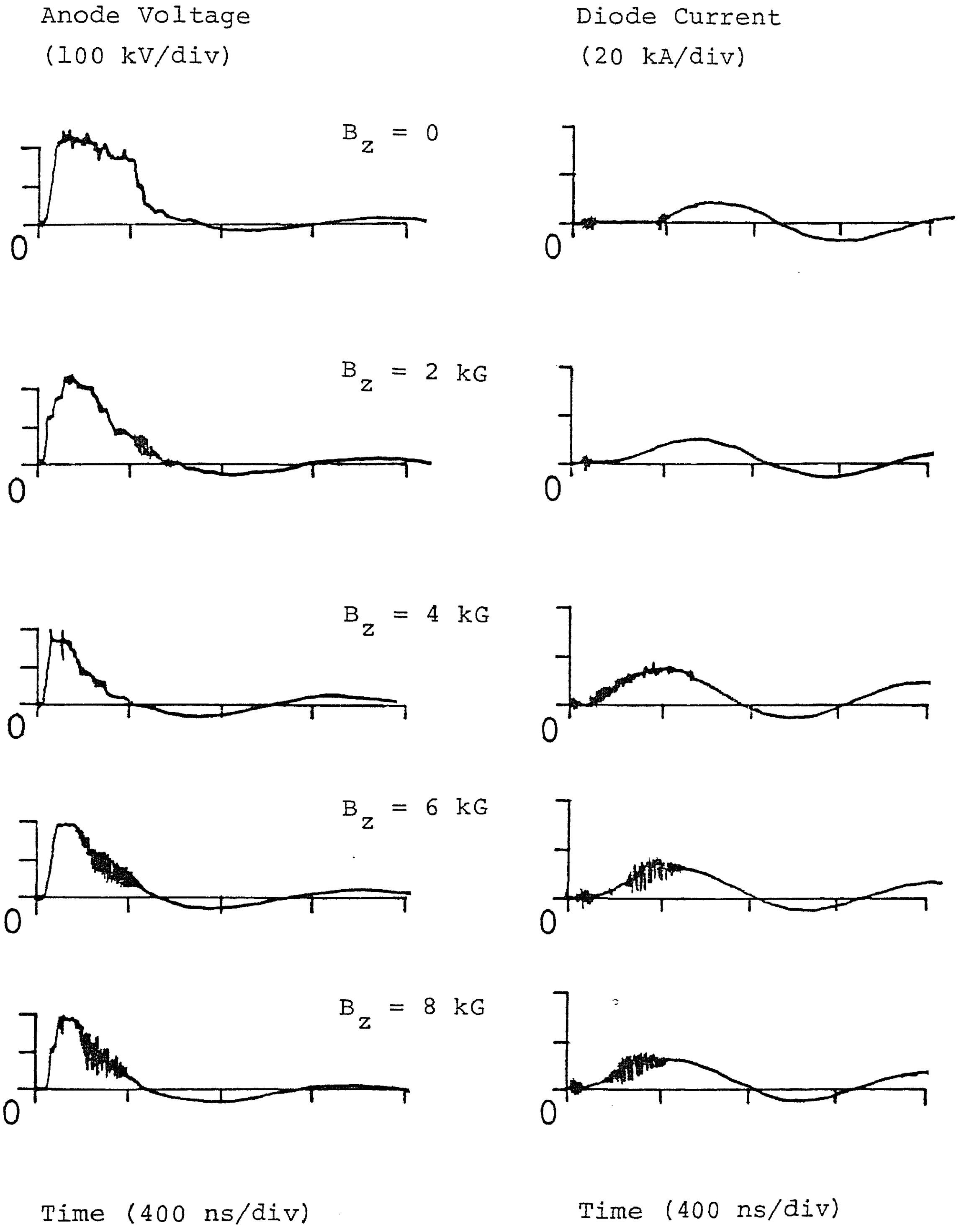
Anode Voltage
(100 kV/div)
Diode Current
(20 kA/div)
$B_z = 0$
$B_z = 2$ kG
$B_z = 4$ kG
$B_z = 6$ kG
$B_z = 8$ kG
0
Time (400 ns/div)
Time (400 ns/div)

Fig. B4

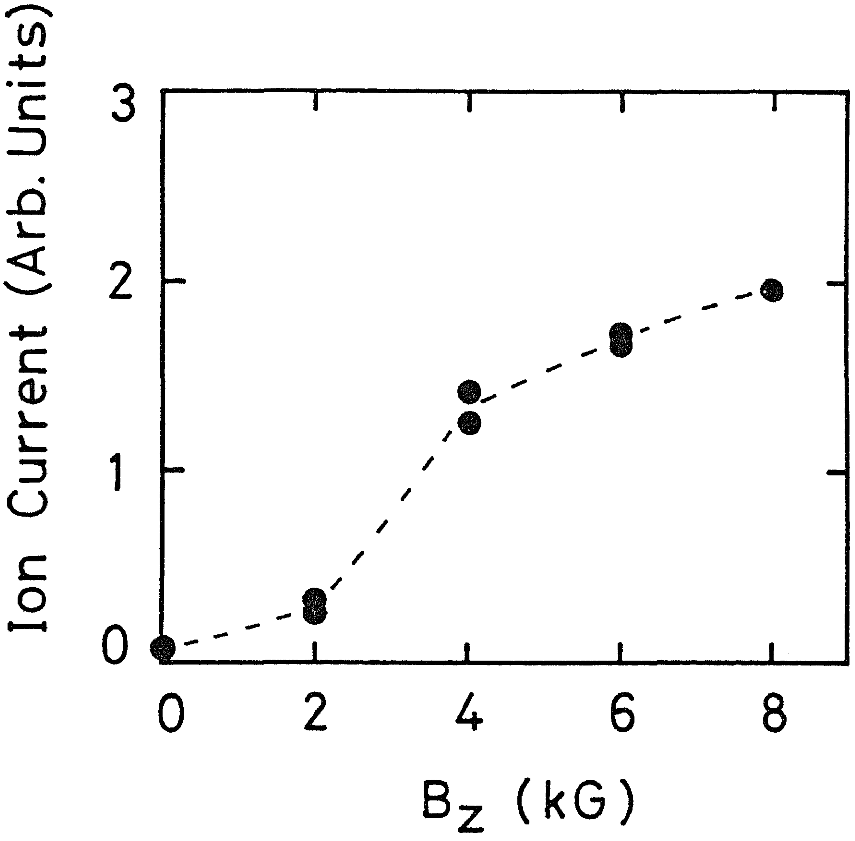

Fig. B5